Supporting Information Appendix

Trichoderma reesei Rad51 tolerates mismatches

in hybrid meiosis with diverse genome sequences

Wan-Chen Li[1,2,3,#], Chia-Yi Lee[4,#], Wei-Hsuan Lan[5,#], Tai-Ting Woo[3,#], Hou-Cheng Liu[3],

Hsin-Yi Yeh[4], Hao-Yen Chang[4], Yu-Chien Chuang[3], Chiung-Ya Chen[3], Chi-Ning Chuang[3],

Chia-Ling Chen[3], Yi-Ping Hsueh[3], Hung-Wen Li[5*], and Peter Chi[4,6*]and Ting-Fang Wang[1,3,*]

[1]Taiwan International Graduate Program in Molecular and Cellular Biology, Academia Sinica,

Taipei 115, Taiwan

[2]Institute of Life Sciences, National Defense Medical Center, Taipei 115, Taiwan

[3]Institute of Molecular Biology, Academia Sinica, Taipei 115, Taiwan

[4] Institute of Biochemical Sciences, National Taiwan University, Taiwan

[5]Department of Chemistry, National Taiwan University, Taiwan

[6]Institute of Biological Chemistry, Academia Sinica, Taipei 115, Taiwan

[#]These authors contributed equally to this work.

[*]Corresponding authors: HWL, email: hwli@ntu.edu.tw; PC, email: peterhchi@ntu.edu.tw;

TFW, email: tfwang@gate.sinica.edu.tw

The supplemental information (SI) file includes "Materials and Method", 18 Supplemental

Tables, 17 Supplemental Figures.

Two dataset files (Dataset S1 and Dataset S2) in Excel format are also provided separately.

MATERIALS AND METHODS

Miscellaneous

Fungal growth, culture media, sexual crossing, single ascospore isolation, preparation of genomic DNA, PCR genotyping, Southern hybridization, DAPI staining and cytological analysis have been described in our previous studies (1, 2). Whole genome sequencing and assembly were carried out according to the PacBio Single Molecule Real-Time (SMRT) method and the Illumina-NextSeq paired-end method (3). Asci were stained with DAPI (4',6-diamidino-2-phenylindole) and visualized using a DeltaVision Core Imaging System (Applied Precision, LLC, USA). In brief, developing or mature perithecia were dissected from the fruiting bodies under a dissection microscope and then soaked in 0.05% Triton™ X-100 with 0.5 µg/ml DAPI. The perithecia were ruptured using Dumont #5 tweezers to release rosettes of asci. Next, the rosettes of asci were carefully aspirated into a pipette tip and released onto a microscope slide for visualization. Fiji ImageJ software was used for image processing.

*Tr*Rad51 monoclonal antibodies were generated using the *Tr*Rad51 proteins (generated as described below) to immunize mice as previously described (4). Budding yeast genetic experiments were performed using S288c/SK1 hybrid diploid strains (5) kindly provided by Alain Nicolas (Institut Curie, CNRS, Paris, France) and Nancy Hollingsworth (Stony brook University, New York, USA). The rabbit anti-Hsp104 antisera were kindly provided by Chung Wang (Academia Sinica, Taiwan) and the goat anti-*Sc*Rad51 antiserum were purchased from Santa Cruz Biotechnology (California, USA).

Pulsed-field gel electrophoresis (PFGE)

Intact chromosomal DNA was prepared using the agarose spheroplasting method with two modifications. The conidia were isolated and germinated in potato dextrose agar (PDA) at 25

°C, 200 rpm for 6 h before being embedded into the agarose plug. *Trichoderma harziaum* lysing enzymes (Sigma-Aldrich Co., St. Louis, MO) were used to digest the cell walls during spheroplasting. Electrophoresis conditions for karyotype analysis were described previously (6).

NGS-based APD calling and mapping of meiotic recombination products

The genomic DNA was isolated from vegetative mycelia of QM6a, CBS999.97(*MAT1-1*), CBS999.97(*MAT1-2*), and the F1 progeny generated by sexually crossing QM6a and CBS999.97(*MAT1-1*), respectively. Next, three different methods were used to quantify and validate the quality of purified genomic DNA (gDNA): (1) NanoDrop 2000 (ThermoFisher Scientific, USA), (2) Qubit 3.0 fluorometer, and (3) Agilent 2200 TapeStation System. Next, the high-quality gDNA was subjected to whole genome sequencing using an Illumina-Miseq sequencer (3).

For variant calling, CLC Genomics Workbench 20.0 (https://digitalinsights.qiagen.com) was used to assemble all genome sequences. MUMmer4 (7) was utilized to genotype APD positions between the four representative F1 progeny relative to either one of the two parental genomes. The results were then analyzed using two publicly available programs [ReCombine (v2.1) (8) and GroupEvents (9)] to detect CO and NCO products. Genotype data were formatted as described previously (5) and the programs were run with a 0 bp threshold (i.e, without grouping closely spaced events). Next, PlotTetrad, a component of the "ReCombine" program (8), was used to create graphical representations of all seven chromosomes of QM6a and CBS999.97(*MAT1-1*).

SNP genotyping and recombination analysis

We have developed a fungus-centric multiple genome sequence alignment (MGSA) tool named "TSETA" [Third-generation Sequencing (TGS) technology Enabled Tetrads Analysis], with two different functional modes: (1) the "SNP" mode is a powerful analytical tool for single-nucleotide-resolution comparisons of different intraspecies genomes; and (2) the "Tetrad" mode enables genome-wide identification of genetic variations before and after a single meiotic event, including meiotic recombination products, illegitimate mutations and repeat-induced point mutation (10, 11). The TSETA source code is publicly available on GitHub (http://github.com/labASIMBTFWang/TSETA) under the GPL-3.0 license.

Assembly of NGS-based genome sequences of 16 F1 progeny

High-quality genomic DNA isolated from each of the 16 F1 progeny was sequenced using an Illumina-NextSeq PE150 system. The resulting *FASTQ* files were applied to the widely-used sequence aligner BWA-MEM (https://arxiv.org/abs/1303.3997; arXiv:1303.3997v2 [q-bio.GN]). using the PacBio genome sequences of the corresponding representative F1 progeny as templates for NGS-based genome assembly. The output SAM files were converted and sorted in SAMTOOLS (12) and then polished in PILON 1.23 (13) using the following commands (--genome reference.fasta, --frags sorted.bam, --fix snps, indels).

Expression plasmids and protein purification

An improved SUMO fusion protein system (14) was used to produce and purify native *Tr*Rad51 proteins in *E. coli*. The *Sc*Rad51 cDNA was cloned into pLant2B vector (15). The *Sc*Dmc1 cDNA was cloned into pNRB150 vector with a hexahistidine (His$_6$) tag and a SUMO tag on the N-terminal (16).

The expression vector for *Tr*Rad51 contained a His$_6$-Smt3-N-terminal tag. The expression plasmid was transformed into the *E. coli* BLR pRAREpLysS strain, a recA$^-$ derivative of BL21

with pRARE to supply tRNAs for rare codons and pLysS to repress basal expression of target genes. The cells were incubated in Luria broth and harvested after 3 h of 1 mM IPTG induction at 37 °C. For protein purification, the cell paste was first suspended with breakage buffer (25 mM Tris-HCl pH 7.5, 10% glycerol, 500 mM KCl, 0.01% Igepal, 2 mM β-mercaptoethanol, 1 mM PMSF, and the protease inhibitors aprotinin, chymostatin, leupeptin, bestatin, and pepstatin A, each at 3 μg/ml), sonicated, and centrifuged. TrRad51 containing supernatant was fractionated in nickel-nitrilotriacetic acid agarose (QIAGEN), followed by on-column Ulp1 digestion, Source Q column (GE Healthcare), macro hydroxyapatite column (GE Healthcare), and Mono Q column (GE Healthcare) purifications. The TrRad51-containing fractions were pooled and concentrated with an Amicon Ultra-30kDa centrifugal filter. All steps were carried out at 4 °C to avoid protein degradation or loss of function, and the concentrated protein was stored at -80 °C.

To express ScRad51, the recA⁻ $E.coli$ BLR pRAREpLysS strain was used with 0.1 mM IPTG induction at 16 °C for 20 h. The purification process of His$_6$-N-terminal-tagged ScRad51 was modified from a previously described procedure (15). In brief, the supernatant of centrifuged cell lysate was precipitated by ammonium sulfate. The dissolved pellet was purified by consecutive chromatographic steps on Sepharose Q, macro hydroxyapatite, and Source Q columns. The expression and purification procedures for ScDmc1 were conducted as previously described (17). Briefly, His$_6$-N-terminal-tagged ScDmc1 was expressed in $E. coli$ Rosetta strain, induced by 1 mM Isopropyl β-d-1-thiogalactopyranoside (IPTG), and then harvested after 3 h incubation in 37 °C. For purification, all buffers contained 0.1 mM Na$_3$VO$_4$, 2 mM ATP and 2 mM MgCl$_2$. Dmc1 was purified through TALON affinity resin (Clontech), a HiTrap Heparin column (GE Healthcare), Ulp1 digestion, and a Mono Q column. The ScRad51- and ScDmc1-containing fractions were processed and stored as described for TrRad51.

DNA substrates

All oligonucleotides without cyanine dyes were purchased from Genomics, whereas oligonucleotides with cyanine dye labels were obtained from Integrated Device Technology. Oligo concentrations were determined by UV absorption in TE buffer (10 mM Tris-HCl pH 8.0, 0.5 mM EDTA) and are reported in the manuscript as nucleotides/base pairs in molar concentration. In the ATPase assay and DNA mobility shift assay, Φx174 viral (+ sense) ssDNA or Φx174 linearized dsDNA was used to stimulate recombinase ATPase activity and binding of protein to DNA was then monitored. To visualize nucleoprotein filaments under electron microscopy, Oligo 1 (5'- TTATGTTCAT TTTTTATATC CTTTACTTTA TTTTCTCTGT TTATTCATTT ACTTATTTTG TATTATCCTT ATCTTATTTA, 80 mer) was mixed with protein.

For the isotope-labeled DNA strand exchange reaction, the ssDNA Oligo 1 was used to form nucleoprotein filament. To prepare the homologous 40-mer donor dsDNA, Oligo 2 (5'- TAATACAAAA TAAGTAAATG AATAAACAGA GAAAATAAAG, 40 mer) was labeled with [γ-P^{32}-ATP] (PerkinElmer) by polynucleotide kinase (New England Biolabs) at the 5' end. Unincorporated [γ-P^{32}-ATP] was removed and then the radiolabeled oligonucleotide was annealed with its exact complementary ssDNA (Oligo 3). The dsDNA duplexes were formed by mixing the same amounts of complementary ssDNA in annealing buffer (50 mM Tris-HCl pH 7.5, 10 mM MgCl$_2$, 100 mM NaCl, 1 mM DTT), and the mixtures were heated up to 85 °C for 3 min and gradually cooled down to room temperature for annealing. The annealed duplex DNA was purified from a 10% polyacrylamide gel and then concentrated for assay.

For D-loop assay, ^{32}P-labeled Oligo 4 (5'- AAATCAATCT AAAGTATATA TGAGTAAACT TGGTCTGACA GTTACCAATG CTTAATCAGT GAGGCACCTA TCTCAGCGAT CTGTCTATTT, 90 mer) and pBluescript supercoiled DNA was used in the

reaction. For fluorescence-based strand exchange, unlabeled Oligo 5 (5-' AAATGAACAT AAAGTAAATA AGTATAAGGA TAATACAAAA TAAGTAAATG AATAAACATA GAAAATAAAG TAAAGGATAT AAA, homologous ssDNA 83 mer) or Oligo 6 (5-' AAATGAACAT AAAGTAAATA AGTATAAGGA TAAT**G**CAAAA TAAGTAAATG AATAAACATA GAAAATAAAG TAAAGGATAT AAA, mismatched ssDNA 83 mer) was used for nucleoprotein filament formation. For homologous donor dsDNA, the substrates were prepared by annealing two ssDNA, i.e., Oligo 7 (5' Cy3- AAATGAACAT AAAGTAAATA AGTATAAGGA TAATACAAAA, 40 mer) with its complementary 3'Cy5-fluorophore-labeled Oligo 8. The annealing steps were described as above.

For Single-Molecule triplex state stability experiments, 3'-biotinylated 5'-Cy5-labeled hybrid DNA was prepared by annealing unlabeled Oligo 9-11 (15-nt full homology, (**15 homo**, TGGCGACGGC AGCGAGGCTT AATTCATCTT CATTATCTCA GTTCTATCAA TCTTAATCTA ATACTCTTAC CTTCCCTCCC TCTGTTTACT ATATTCTTA), 15-nt containing 1 mismatch (**15 mis**, TGGCGACGGC AGCGAGGCTT AATTCATCTTCA TTATCTCAGT TCTATCAATC TTAATCTAAT ACTCTTACCT TCCCACCCTC TGTTTACTATA TTCTTA) and 12-nt full homology (**12 homo**, TGGC GACGGC AGCGAGGCTT AATTCATCTT CATTATCTCA GTTCTATCAA TCTTAATCTA ATACTCTTAC CTTCCCTCAT ACTGTTTACT ATATTCTTA)) with Oligo 12 (5'Cy5-GCCTCGCTGC CGTCGCCA-3'bio, 3'-biotinylated 5'-Cy5-labeled 18-nt ssDNA) at 1.2:1 ratio. To prepare Cy3-labeled 40-bp dsDNA, Oligo 13 (5'Cy3-TTCAGGGAGG GAAGGTAATT TTTGTTTTTT ATTTTTTTTT) and its complementary unlabeled Oligo 14 was annealed at 1:1.2 ratio.

ATPase assay

All indicated concentrations for ATPase assays represent final concentrations, and all reactions were repeated three times. TrRad51 (2.5 μM) was incubated in buffer A (35 mM Tris-HCl pH 7.5, 1 mM DTT, 50 mM KCl, 0.25 mM MgCl$_2$, 0.1 mg/mL BSA, 1 mM ATP and 0.6 μCi [γ-P^{32}-ATP]) with or without Φx174 viral (+ sense) ssDNA (37.5 μM) or linearized dsDNA (37.5 μM) at 37 °C for the indicated times. At each indicated time-point, 2 μl of reaction mixture was mixed with an equal volume of 500 mM EDTA. ATPase activity was determined by thin-layer chromatography on a polyethyleneimine sheet (Sigma-Aldrich), with 0.15 M LiCl and 0.5 M formic acid as the developing buffer. The polyethyleneimine sheet was then air-dried and scanned with a phosphorimager (Bio-Rad).

DNA mobility shift assay

A fixed amount of Φx174 viral (+ sense) ssDNA (15 μM) or Φx174 linearized dsDNA (15 μM) was incubated with indicated amounts of TrRad51 in buffer B (35 mM Tris-HCl pH 7.5, 1 mM DTT, 50 mM KCl, 0.25 mM MgCl$_2$, 1 mM ATP, and 0.1 mg/mL BSA) at 30 °C for 5 min. The reaction mixtures were separated by 1% agarose gel electrophoresis in TBE buffer (89 mM Tris-HCl pH 8.0, 89 mM Boric acid, 2 mM EDTA) at 4 °C. The gel was stained with SYB Gold Nucleic Acid Gel Stain (Invitrogen) and analyzed using a gel documentation station (Bio-Rad).

Negative-staining electron microscopy

Reaction mixtures were assembled with combinations of 0.8 μM TrRad51 with 80-mer Oligo (2.4 μM nucleotides) in 12.5 μl of buffer B without BSA, with 10 mM CaCl$_2$, at 30 °C. After 30 min incubation, 4 μl of reaction was applied onto 400-mesh grids coated with fresh carbon film that had been glow-discharged. Samples were stained with 2% uranyl acetate for 1 min

and examined in a Hitach H-7100 transmission electron microscope operated at 75 keV in conjunction with a CCD camera at a nominal magnification (50,000 or 200,000X).

DNA strand-exchange assay

All the reaction steps were carried out at 30 °C. The 80-mer Oligo 1 (4.8 μM) was incubated with the indicated amounts of *Tr*Rad51 protein in buffer B, with or without 10 mM $CaCl_2$ for 5 min. Addition of ^{32}P-labeled 40-mer homologous duplex (2.4 μM) initiated the reaction, which lasted for 30 min unless indicated otherwise. A 5 μl aliquot was extracted and mixed with an equal volume of 0.1% SDS and 1 mg/ml proteinase K, before being incubated at 37 °C for 15 min. The reaction mixtures were separated with 10% polyacrylamide gels in TBE buffer at 4 °C. The gel was dried and scanned with a phosphorimager. For concentration titration, we used 0.8, 1.6, 2.4 and 4.8 μM of *Tr*Rad51. For time-course analysis, we executed a 5-, 10-, 15- and 30-min incubation after addition of dsDNA.

D-loop assay

All reaction steps were carried out at 30 °C. The ^{32}P-labeled 90-mer Oligo 4 (2.4 μM) was pre-incubated with *Tr*Rad51 in buffer B containing 10 mM $CaCl_2$ for 5 min, followed by addition of pBluescript dsDNA (37 μM) to initiate the D-loop reaction. After a 30-min incubation, a 5 μl aliquot was removed and mixed with an equal volume of 0.2% SDS and 0.8 mg/ml proteinase K, before incubation for 15 min. After electrophoresis in a 0.85 % agarose gel in TBE buffer, the gel was dried onto DE81 paper for visualization and quantification of the radiolabeled DNA species by phosphorimaging. For concentration titration, 0.2, 0.4, 0.8 and 1.6 μM of *Tr*Rad51 were used. For time-course analysis, we executed a 5-, 10-, 15- and 30-min incubation after the addition of pBluescript dsDNA.

Fluorescence-based strand exchange

Homologous Oligo 5 or mismatched Oligo 6 (3 μM nucleotides) was first pre-incubated with recombinases (1 μM) to assemble nucleoprotein complex in recombinase reaction buffer (buffer B containing 10 mM $CaCl_2$ for TrRad51; buffer C for ScRad51: 35 mM Tris-HCl pH 7.5, 1 mM DTT, 15 mM KCl, 2.5 mM $MgCl_2$, 1 mM Spermine, 1 mM ATP, and 0.1 mg/mL BSA; buffer D for ScDmc1: 35 mM Tris-HCl pH 7.5, 1 mM DTT, 50 mM KCl, 2.5 mM $MgCl_2$, 0.5 mM $CaCl_2$, 1 mM ATP, and 0.1 mg/mL BSA) at 4 °C for 30 min. The addition of homologous dsDNA (Oligo 7+8; 1.45 μM base pairs) initiated the strand exchange reaction. The reaction mixture was transferred into Falcon 384-well Black/Clear flat plates at room temperature, and then emission signal of Cy3 at 590 nm in the reaction mixture was detected using a BioTek SynergyHTX multi-mode reader every 2 min for 120 min.

In the reaction mixture undergoing DNA strand exchange, the two strands of donor dsDNA separate, causing an increase in Cy3 emission signal. The emission signal (F_t) at 590 nm for each time-point was calculated using the following equation: $F_t = (S_t - S_0) - (B_t - B_0)$ where "S_t" is the fluorescence emission at 590 nm in the reaction containing recombinase at a given time-point, "B_t" is the fluorescence emission at 590 nm in the reaction without recombinase at a given time-point, and "S_0" and "B_0" are the fluorescence emissions at 590 nm at the beginning of reactions with or without proteins, respectively. The emission signal is then normalized with the strongest signal in each group. Relative strand exchange efficiency (R_f shown as %) to represent mismatch tolerance is calculated using the following equation: $R_f = F_M / F_H$ where "F_M" is the 590 nm emission signal (F_t) at the 120 min time-point of the reaction with mismatched substrates, and "F_H" is the 590 nm emission signal of the reaction with homologous substrates at the 120 min time-point. The significance between mismatch tolerance of recombinases was analyzed with GraphPad Prism 7. The Shapiro-Wilk normality

test was performed to test if the data was normally distributed. All groups were compared using one-way ANOVA with Tukey's post hoc test.

Single-molecule triplex state stability experiments and data analysis

The reaction was conducted by incubating 0.02 mg/mL streptavidin for 5 min on a PEGylated slide and coverslip, prepared as previously described (18). After washing away excess streptavidin using buffer F (20 mM Tris-HCl and 50 mM NaCl), the 3'-biotinylated Cy5-labeled hybrid DNA was immobilized on the streptavidin-coated surface for 5 min. Free hybrid DNA was flushed away using recombinase reaction buffer (as described in the section on Fluorescence-based strand exchange) in the presence of imaging buffer G components (4 mg/mL glucose, 30 U/mL glucose oxidase, 30 U/mL catalase, 1 mM dithiothreitol, and 1 mg/mL BSA). Then, the recombinase (1 μM *Tr*Rad51, 1 μM *Sc*Rad51 or 2 μM *Sc*Dmc1) with 2 mM ATP, 1 mM dithiothreitol and 1 mg/mL BSA in recombinase reaction buffer was incubated with surface-bound hybrid DNA for 15 min to form nucleoprotein filaments. After washing away excess recombinase, triplex state formation was initiated by introducing 10 nM Cy3-labeled 40 bp double-stranded DNA (representing either 15-nt full homology, 12-nt full homology or 15-nt with 1-nt mismatched sequence at the 11th position) into the reaction chamber for 20 min. On average, we observed approximately 29.3 ±11.4 Cy3-Cy5 co-localized spots (mean ±S.D.). We controlled for surface density and scored co-localization solely within 6 pixels of the anchored Cy5-labeled strand so that specific co-localization was counted. Attempting to map the Cy3-labeled dsDNA spots onto a different and incorrect field-of-view of the Cy5-labeled anchored strands returned only ~2.7 ±0.6 spots. Control experiments containing no recombinases returned only ~0.4 ±0.5 co-localized spots, confirming that co-localized spots in our experiments are recombinase-mediated triplex states. Free Cy3-labeled

40 bp double-stranded DNA was then flushed away using imaging buffer G with 2 mM ATP, and this time-point was defined as time zero.

We utilized an objective-type total internal reflection fluorescence microscope (IX2; Olympus) equipped with 532-nm and 633-nm lasers to alternatively excite the Cy3 and Cy5 dyes. Mapping of the Cy3 and Cy5 imaging channels was achieved using mapping oligos containing annealed Cy3-labeled oligo and biotinylated Cy5-labeled oligo, respectively, based on a mapping algorithm written in MATLAB (19). The fluorescent signal was acquired by an electron-multiplying CCD system (ProEM 512B; Princeton Instruments) at 10 Hz for 20-frames (2-second) for 532-nm and 633-nm excitation each at given time-points using a dual-view system. Laser excitation was switched off between given time-points. Under the experimental conditions we used (including laser power and camera exposure time), less than 10% of Cy3 dyes photobleach after 60-sec continuous excitation. Image acquisition was achieved using a program written in LABVIEW 8.6. Automatic spot detection and colocalization analysis was performed using MATLAB. Data points shown are from at least three independent experiments and error bars represent standard error of the mean.

Table S1. List of all *Trichoderma reesei* strains analyzed by PacBio RSII or Illumina-NextSeq whole genome sequencing technology

Strain	Description	Sequencing platform	BioProject accession	WGS/SRA accession
QM6a	wild type QM6a	PacBio RSII	PRJNA325840	CP016232-CP016238
CBS999.97(*MAT1-1*)	Wild type (*MAT1-1*)	PacBio RSII	PRJNA352653	CP017983-CP017984, CP020875-CP020879
CBS999.97(*MAT1-2*)	Wild type (*MAT1-2*)	PacBio RSII	PRJNA382020	CP020724-CP020730
#1-1	The #1 ascospore in the #1 QM6a/CBS999.97(MAT1-1) ascus	ILLUMINA NextSeq 500	PRJNA433292	SRR6884669
#1-1	The #1 ascospore in the #1 QM6a/CBS999.97(MAT1-1) ascus	PacBio RSII	PRJNA386077	CP021290-CP021296
#1-2	The #2 ascospore in the #1 QM6a/CBS999.97(MAT1-1) ascus	ILLUMINA NextSeq 500	PRJNA433292	SRR6884668
#1-3	The #3 ascospore in the #1 QM6a/CBS999.97(MAT1-1) ascus	ILLUMINA NextSeq 500	PRJNA433292	SRR6884667
#1-3	The #3 ascospore in the #1 QM6a/CBS999.97(MAT1-1) ascus	PacBio RSII	PRJNA386077	CP021297-CP021303
#1-4	The #4 ascospore in the #1 QM6a/CBS999.97(MAT1-1) ascus	ILLUMINA NextSeq 500	PRJNA433292	SRR6884666
#1-5	The #5 ascospore in the #1 QM6a/CBS999.97(MAT1-1) ascus	ILLUMINA NextSeq 500	PRJNA433292	SRR6884673
#1-6	The #6 ascospore in the #1 QM6a/CBS999.97(MAT1-1) ascus	ILLUMINA NextSeq 500	PRJNA433292	SRR6884672
#1-7	The #7 ascospore in the #1 QM6a/CBS999.97(MAT1-1) ascus	ILLUMINA NextSeq 500	PRJNA433292	SRR6884671
#1-7	The #7 ascospore in the #1 QM6a/CBS999.97(MAT1-1) ascus	PacBio RSII	PRJNA386077	CP021304-CP021310
#1-8	The #8 ascospore in the #1 QM6a/CBS999.97(MAT1-1) ascus	ILLUMINA NextSeq 500	PRJNA433292	SRR6884670
#1-9	The #9 ascospore in the #1 QM6a/CBS999.97(MAT1-1) ascus	ILLUMINA NextSeq 500	PRJNA433292	SRR6884665
#1-10	The #10 ascospore in the #1 QM6a/CBS999.97(MAT1-1) ascus	ILLUMINA NextSeq 500	PRJNA433292	SRR6884664

#1-11	The #11 ascospore in the #1 QM6a/CBS999.97(MAT1-1) ascus	ILLUMINA NextSeq 500	PRJNA433292	SRR6884649
#1-11	The #11 ascospore in the #1 QM6a/CBS999.97(MAT1-1) ascus	PacBio RSII	PRJNA386077	CP021311-CP021317
#1-12	The #12 ascospore in the #1 QM6a/CBS999.97(MAT1-1) ascus	ILLUMINA NextSeq 500	PRJNA433292	SRR6884648
#1-13	The #13 ascospore in the #1 QM6a/CBS999.97(MAT1-1) ascus	ILLUMINA NextSeq 500	PRJNA433292	SRR6884651
#1-14	The #14 ascospore in the #1 QM6a/CBS999.97(MAT1-1) ascus	ILLUMINA NextSeq 500	PRJNA433292	SRR6884650
#1-15	The #15 ascospore in the #1 QM6a/CBS999.97(MAT1-1) ascus	ILLUMINA NextSeq 500	PRJNA433292	SRR6884653
#1-16	The #16 ascospore in the #1 QM6a/CBS999.97(MAT1-1) ascus	ILLUMINA NextSeq 500	PRJNA433292	SRR6884652
#2-1	The #1 ascospore in the #2 QM6a/CBS999.97(MAT1-1) ascus	ILLUMINA NextSeq 500	PRJNA433292	SRR6884655
#2-5	The #5 ascospore in the #2 QM6a/CBS999.97(MAT1-1) ascus	ILLUMINA NextSeq 500	PRJNA433292	SRR6884654
#2-9	The #9 ascospore in the #2 QM6a/CBS999.97(MAT1-1) ascus	ILLUMINA NextSeq 500	PRJNA433292	SRR6884647
#2-13	The #13 ascospore in the #2 QM6a/CBS999.97(MAT1-1) ascus	ILLUMINA NextSeq 500	PRJNA433292	SRR6884646
#3-1	The #1 ascospore in the #3 QM6a/CBS999.97(MAT1-1) ascus	ILLUMINA NextSeq 500	PRJNA433292	SRR6884642
#3-5	The #5 ascospore in the #3 QM6a/CBS999.97(MAT1-1) ascus	ILLUMINA NextSeq 500	PRJNA433292	SRR6884643
#3-9	The #9 ascospore in the #3 QM6a/CBS999.97(MAT1-1) ascus	ILLUMINA NextSeq 500	PRJNA433292	SRR6884644
#3-13	The #13 ascospore in the #3 QM6a/CBS999.97(MAT1-1) ascus	ILLUMINA NextSeq 500	PRJNA433292	SRR6884645

Table S2. Summary of PacBio RSII sequencing and assembly results

Strain		QM6a[1]	CBS999.97(*MAT1-1*)	CBS999.97(*MAT1-2*)
Total sequenced bases		3,397,762,180 bp	4,810,795,008 bp	6,202,644,396 bp
Maximum of all assembled unitigs		6,835,650 bp	6,822,671 bp	6,835,650 bp
N_{50} of all assembled unitigs		5,311,312 bp	5,258,125 bp	5,262,578 bp
Number of reads		263,312	370,345	636,376
N_{50} reads		18,236 bp	18,599 bp	14,406 bp
Phred Quality Score (Q)[2]		48.8	48.1	48.7
Unitigs		7 linear chromosomes	7 linear chromosomes	7 linear chromosomes
Coverage		81X	93X	127X
Genome size		34,922,528 bp	34,319,199 bp	34,324,311 bp
Unidentified bases (N)		0 bp	0 bp	0 bp
GC content		51.1%	51.6%	51.6%
Mitochondria genome (circular)		42139	39004	39004
BUSCO Metrics (Genome)[3]	Total	100%	98.5%	98.4%
	Single complete (S); Duplicated complete (D); Fragment (F); Missing (M)	S:100%; D:0.0%; F:0.0%; M:0.0%	S:98.3%; D:0.2%; F:0.8%; M:0.7%	S:98.3%; D:0.1%; F:0.8%; M:0.8%
BUSCO metrics (Protein)[4]	Total	96.8%	98.8%	98.3%
	Single complete (S); Duplicated complete (D); Fragment (F); Missing (M)	S:96.6%; D:0.2%, F:3.0%; M:0.2%	S:98.6%,D:0.2%, F:0.9%,M:0.3%	S:98.1%; D:0.2%; F:1.3%; M:0.4%

1. The nuclear and mitochondrial genome sequences was reported previously(3). The genome sequence and the original genome-wide annotation data are publicly available (https://mycocosm.jgi.doe.gov/Trire_Chr/Trire_Chr.home.html).
2. Phred Quality Score (Q) is a measure of the quality of the identification of the nucleotide sequences generated by automated DNA sequencing (20).
3. To quantitatively measure genome assembly completeness, we have applied BUSCO (https://busco.ezlab.org), an open-source software with a large selection of lineage-specific sets of Benchmarking Universal Single-Copy Orthologs(21).
4. Evolutionarily-informed expectations of gene content from near-universal single-copy orthologs is selected from OrthoDB (https://www.orthodb.org) (22).
5. The *Funannotate* v1.5.3 pipeline (23) was applied to (re)annotate the genome sequences of QM6a, CBS999.97(*MAT1-1*) and CBS999.97(*MAT1-2*) (this study). We then applied BUSCO(3) again to quantitatively measure annotation completeness based on the evolutionarily-informed expectations of gene content from near-universal single-copy orthologs from OrthoDB (22).

Table S3. Characteristics and assembly of the seven CBS999.97 chromosomes

Strain	Chromosome	Size (bp)	GC (%)[1]	N[2]	Centromere[3]	[4]Telomeric repeats L	[4]Telomeric repeats R	L telomere + subtelomere[5] / R telomere + subtelomere[5]
CBS999.97(*MAT1-1*)	I	6,822,680	52.09	0	3184500- 3359500 (~175 kb)	12	10	1-19500
								6812500-6822680
	II	5,559,498	52.40	0	1892000-2063500 (~172 kb)	10	10	1-4000
								5558500-5559498
	III	5,258,134	52.11	0	1677500-1830500 (~153 kb)	13	10	1-4000
								5256000-5258134
	IV	4,872,985	52.06	0	1453500- 1617500 (~164 kb)	13	9	1-1500
								4842500-4872985
	V	4,096,940	51.81	0	1102500-1259500 (~157 kb)	8	13	1-17500
								4092500-4096940
	VI	3,741,771	50.24	0	1636500-1810000 (~174 kb)	--	9	1-32500
								3741000-3741771
	VII	3,967,191	49.80	0	1858000-2018500 (~161 kb)	12	9	1-30000
								3956000-3967191
	Overall	34,319,199	51.6	0	1071500 bp	68	70	~157 kb

CBS999.97(*MAT1-2*)	I	6,822,679	52.09	0	3184500- 3359500 (~175 kb)	14	7	1-19500
								6814000-6822679
	II	6,061,978	52.37	0	1892000-2063500 (~172 kb)	12	12	1-4000
								6042500-6061978
	III	5,262,578	52.11	0	1677500-1830500 (~153 kb)	14	7	1-4000
								5256000-5262578
	IV	4,370,647	52.07	0	1453500- 1617500 (~164 kb)	8	13	1-1500
								4369500-4370647
	V	4,096,893	51.81	0	1102500-1259500 (~157 kb)	10	7	1-17500
								4092500-4096893
	VI	3,742,327	50.23	0	1637000-1810500 (~174 kb)	-	13	1-33000
								3741500-3742327
	VII	3,927,209	49.80	0	1858000-2018500 (~161 kb)	8	14	1-30000
								3956000-3967209
	Overall	34,324,311	51.6	0	1153000 bp	66	73	~157 kb

1. The EMBOSS geecee tool (http://www.bioinformatics.nl/cgi-bin/emboss/geecee) was used to calculate the fractional GC content using a 500 bp sliding window.
2. Number of unresolved bases (N).
3. Centromeres were manually identified as the longest AT-rich islands in each chromosome.
4. The telomeric repeats were identified as $(TTAGGG)_n$ at 3′ termini and the complementary sequence $(CCCTAA)_n$ at 5′ termini.
5. Subtelomeres were manually identified as the AT-rich island right next to the telomeric repeats.

Table S4. Transposable elements in QM6a(1), CBS999.97(*MAT1-1*) and CBS999.97(*MAT1-2*)

Strain	Genome size (bp)	Repetitive sequences (bp)	Overall	Class I (retrotransposons)							Class II (transposons)					Others
				Tad1-LINE	*I*-LINE	*Jockey*-LINE	other LINEs	*Copia*-LTR	*Gypsy*-LTR	other LTRs	*CMC-EnSpm*	*hAT*	*MULE-MuDR*	*TcMar -Fot1*	*PIF-Harbinger-like*	
				copy number												
QM6a	34922528	42035	70	0	0	4	14	8	10	4	6	0	21	0	0	3
CBS999.97 (*MAT1-1*)	34319199	20756	62	0	0	11	11	5	2	6	4	1	17	0	0	5
CBS999.97 (*MAT1-2*)	34324311	20756	62	0	0	11	11	5	2	6	4	1	17	0	0	5

Table S5. Size distribution of AT-rich blocks in QM6a(3), CBS999.97(*MAT1-1*) and CBS999.97(*MAT1-2*)

Strain	Genome (Mb)	Chromosome number	GC (%)	Number of AT-rich blocks of different lengths (L in kb)[1]									
				$0.5 \leq L < 1$	$1 \leq L < 3$	$3 \leq L < 5$	$5 \leq L < 10$	$10 \leq L < 15$	$15 \leq L < 20$	$20 \leq L < 50$	$50 \leq L < 100$	$L > 100$	Total
QM6a	34.9	7	51.1 ± 11.6	1845	337	69	38	26	13	9	6	6	2249
CBS999.97(*MAT1-1*)	34.3	7	51.6 ± 10.7	1861	272	51	23	20	10	10	7	5	2259
CBS999.97(*MAT1-2*)	34.3	7	51.6 ± 10.8	1826	301	50	21	20	9	10	8	5	2250

1.AT-rich interspersed islands were identified by their AT contents being ≥6% higher than that of average DNA in each fungal genome.

Table S6. APDs between QM6a and CBS999.97(*MAT1-1*)

Chromosome	MUMmer4			TSETA (SNP mode)		
	APDs	SNPs	InDels	APDs	SNPs	InDels
I	188729	120810	67919	928283	231152	697131
II	159995	102547	57448	1254388	172968	1081420
III	136910	88503	48407	622873	157654	465219
IV	122867	78085	44782	1120822	131911	988911
V	115253	72582	42671	565759	164166	401593
VI	104773	70501	34272	968639	132073	836566
VII	107472	71550	35922	697216	148655	548561
Genome	935999	604578	331421	6157980	1138579	5019401

Table S7. APDs between QM6a and CBS999.97(*MAT1-2*)

Chromosome	APDs	SNPs	InDels
I	188658	120800	67858
II	173152	110865	62287
III	136994	88518	48476
IV	123284	78370	44914
V	115260	72579	42681
VI	104620	70258	34362
VII	107480	71557	35923
Genome	949448	612947	336501

Table S8. APDs between CBS999.97(*MAT1-1*) and CBS999.97(*MAT1-2*)

Chromosome	APDs	SNPs	InDels
I	404	73	331
II	325	116	209
III	616	301	315
IV	265	43	222
V	271	79	192
VI	474	147	327
VII	350	180	170
Genome	2705	939	1766

Table S9A. Application of the NGS-based approach to detect the CO products generated by QM6a and CBS999.97(*MAT1-1*) hybrid meiosis

Asci number	Chromosome number	Chromatids	APD_start_out	APD_start_in	APD_end_in	APD_end_out	Position of CO[1]	GC tract associated with CO	GC tract length[2] (bp)	CO length (bp)	snpmarker in GC	snp number in GC of TSETA	#snp / GC length
1	1	[1,4]	290360	290417	290660	290742	290545	yes	313	313	5	5	0.016
1	1	[1,4]	1376466	1376630	1376220	1376316	1376408	yes	280	280	3	5	0.018
1	1	[3,4]	2846520	2846712	2846520	2846712	2846616	no	0	192	0	0	-
1	1	[1,3]	4850040	4850203	4850040	4850203	4850122	no	0	163	0	0	-
1	1	[2,4]	5942600	5942621	5942621	5942690	5942633	yes	45	45	1	1	0.022
1	2	[3,4]	1078135	1078229	1078313	1078580	1078314	yes	265	265	5	5	0.019
1	2	[1,2]	3067988	3068061	3067677	3067793	3067880	yes	290	290	6	6	0.021
1	2	[1,2]	4581140	4581413	4581140	4581413	4581277	no	0	273	0	0	-
1	3	[1,4]	389234	389285	389129	389234	389221	yes	78	78	1	1	0.013
1	3	[2,4]	1639259	1639497	1639199	1639259	1639304	yes	149	149	1	1	0.007
1	3	[1,3]	2230660	2231098	2230660	2231098	2230879	no	0	438	0	0	-
1	4	[1,3]	823701	823776	823701	823776	823739	no	0	75	0	0	-
1	4	[1,2]	1922088	1922223	1921803	1921929	1922011	yes	290	290	6	6	0.021
1	4	[1,2]	3937229	3937528	3937528	3937598	3937471	yes	185	185	1	1	0.005
1	5	[3,4]	906203	906347	906347	906371	906317	yes	84	84	1	1	0.012
1	5	[3,4]	1651260	1651328	1651328	1651483	1651350	yes	112	112	1	2	0.018
1	5	[2,3]	2640809	2641088	2640737	2640809	2640861	yes	176	176	1	1	0.006
1	5	[1,3]	3964850	3965199	3964850	3965199	3965025	no	0	349	0	0	-
1	6	[1,2]	640643	640693	640864	641090	640823	yes	309	309	6	6	0.019

1	6	[2,4]	2245618	2246094	2245618	2246094	2245856	no	0	476	0	0	-
1	6	[1,3]	3265860	3266018	3266018	3266194	3266023	yes	167	167	1	1	0.006
1	7	[3,4]	1180585	1180958	1180585	1180958	1180772	no	0	373	0	0	-
1	7	[1,2]	2890900	2890971	2891551	2891642	2891266	yes	661	661	6	6	0.009
1	7	[3,4]	3411387	3411435	3411632	3411692	3411537	yes	251	251	15	15	0.060
2	1	[1,2]	442558	442580	442608	442895	442660	yes	183	183	3	3	0.016
2	1	[1,2]	1506474	1506720	1506745	1506803	1506686	yes	177	177	2	2	0.011
2	1	[1,3]	2084691	2084737	2084691	2084737	2084714	no	0	46	0	0	-
2	1	[2,3]	4251294	4251404	4251501	4251936	4251534	yes	370	370	3	3	0.008
2	1	[1,2]	5974725	5974980	5974725	5974980	5974853	no	0	255	0	0	-
2	2	[2,4]	1674268	1674949	1674268	1674949	1674609	no	0	681	0	0	-
2	2	[2,4]	3360922	3361041	3361146	3361272	3361095	yes	228	228	2	2	0.009
2	2	[1,2]	4300767	4301025	4300364	4300510	4300667	yes	459	459	8	8	0.017
2	2	[2,3]	5020085	5020184	5019921	5020071	5020065	yes	139	139	2	6	0.043
2	3	[1,2]	514260	514334	514359	514393	514337	yes	79	79	5	5	0.063
2	3	[1,3]	1423196	1423241	1423196	1423241	1423219	no	0	45	0	0	-
2	3	[1,3]	2307852	2308078	2307631	2307774	2307834	yes	263	263	3	3	0.011
2	3	[3,4]	3159300	3159525	3159300	3159525	3159413	no	0	225	0	0	-
2	4	[2,4]	575839	575922	575839	575922	575881	no	0	83	0	0	-
2	4	[2,4]	2627285	2627293	2627636	2627691	2627476	yes	375	375	9	14	0.037
2	4	[2,4]	4085711	4085902	4085543	4085711	4085717	yes	180	180	1	1	0.006
2	5	[1,3]	745152	745275	745152	745275	745214	no	0	123	0	0	-
2	5	[1,3]	1724856	1725224	1724856	1725224	1725040	no	0	368	0	0	-
2	5	[1,2]	3666820	3666825	3666742	3666820	3666802	yes	42	42	1	1	0.024
2	6	[2,3]	833048	833157	832423	832694	832831	yes	544	544	13	17	0.031
2	6	[2,4]	3013333	3013564	3012895	3012955	3013187	yes	524	524	6	41	0.078
2	7	[2,3]	1243420	1243724	1243241	1243413	1243450	yes	245	245	3	26	0.106

2	7	[2,3]	2211545	2211672	2211545	2211672	2211609	no	0	127	0	0	-
2	7	[3,4]	3111332	3111536	3110921	3111076	3111216	yes	436	436	7	30	0.069
3	1	[2,3]	250116	250612	250965	251305	250750	yes	771	771	2	3	0.004
3	1	[1,2]	801334	801348	801334	801348	801341	no	0	14	0	0	-
3	1	[1,3]	2704304	2704336	2704501	2704569	2704428	yes	215	215	8	8	0.037
3	1	[2,4]	5831517	5831622	5831664	5831925	5831682	yes	225	225	3	3	0.013
3	2	[1,3]	422994	423160	423367	423632	423288	yes	423	423	4	4	0.009
3	2	[2,3]	1529079	1529171	1518542	1518568	1523840	yes	10570	10570	158	1590	0.150
3	2	[2,3]	1673723	1673857	1673488	1673564	1673658	yes	264	264	5	4	0.015
3	2	[2,3]	2537986	2538219	2537835	2537976	2538004	yes	197	197	2	2	0.010
2	2	[2,3]	3335826	3336217	3335826	3336217	3336022	no	0	391	0	0	-
3	2	[2,3]	5223023	5223642	5223023	5223642	5223333	no	0	619	0	0	-
3	3	[1,2]	537260	537458	537260	537458	537359	no	0	198	0	0	-
3	3	[2,4]	1395209	1395432	1395209	1395432	1395321	no	0	223	0	0	-
3	3	[1,3]	2086346	2086547	2085628	2085849	2086093	yes	708	708	7	7	0.010
3	4	[1,4]	557846	558182	557846	558182	558014	no	0	336	0	0	-
3	4	[1,4]	1902383	1902552	1901961	1902383	1902320	yes	296	296	1	1	0.003
3	4	[1,2]	2676737	2676891	2676737	2676891	2676814	no	0	154	0	0	-
3	4	[1,2]	3558403	3558505	3557186	3557217	3557828	yes	1253	1253	12	33	0.026
3	5	[2,3]	776022	776148	775763	775830	775941	yes	289	289	6	14	0.048
3	5	[2,4]	1672597	1672807	1672372	1672594	1672593	yes	219	219	2	21	0.096
3	5	[1,3]	2923773	2923934	2923997	2924060	2923941	yes	175	175	3	3	0.017
3	5	[2,4]	3952992	3953332	3952992	3953332	3953162	no	0	340	0	0	-
3	6	[2,4]	600880	600918	600933	601023	600939	yes	79	79	2	2	0.025
3	6	[2,4]	1444127	1444280	1444280	1444692	1444345	yes	283	283	1	9	0.032
3	6	[2,4]	2581058	2581227	2581227	2581576	2581272	yes	259	259	1	1	0.004
3	6	[2,4]	3091487	3091546	3090941	3091107	3091270	yes	493	493	7	25	0.051

| 3 | 7 | [1,3] | 1092936 | 1093155 | 1092699 | 1092936 | 1092932 | yes | 228 | 228 | 1 | 1 | 0.004 |
| 3 | 7 | [2,3] | 3110158 | 3110271 | 3109955 | 3110158 | 3110136 | yes | 158 | 158 | 1 | 139 | 0.880 |

[1]Position was defined as the average of APD_start_out, APD_start_in, APD_end_in, APD_end_out

[2]GC tract length were the average of distances between (APD_end_out, APD_start_out) and the distance between (APD_end_in, APD_end_out)

Table S9B. Application of the NGS-based approach to detect the NCO products (with >2 3:1 and/or 4:0 markers) generated by QM6a and CBS999.97(*MAT1-1*) hybrid meiosis

Asci number	Chromosome number	Chromatids	APD_start_out	APD_start_in	APD_end_in	APD_end_out	Position of NCO	GC tract length (bp)	APD marker	NCO length
1	1	4	2841732	2841773	2841798	2842041	2841836	167	2	167
1	2	1	1379241	1379363	1379405	1379528	1379384	164.5	3	165
1	3	3	1308011	1308088	1308375	1308402	1308219	339	22	339
1	3	2	1581077	1581212	1581214	1581307	1581203	116	2	116
1	3	2	3934647	3934821	3935580	3935970	3935255	1041	13	1041
1	3	1	4101219	4101426	4101619	4101796	4101515	385	9	385
1	5	1	783355	783388	783475	783607	783456	169.5	2	170
1	5	1	2906100	2906222	2906235	2906367	2906231	140	3	140
1	6	1	2041331	2042652	2042737	2042764	2042371	759	2	759
2	1	3	1369629	1370048	1370056	1370333	1370017	356	2	356
2	1	2	3651786	3651791	3651837	3651856	3651818	58	3	58
2	1	4	3712241	3712365	3712549	3712728	3712471	335.5	12	336
2	2	1	1084839	1084945	1085158	1085167	1085027	270.5	8	271
2	2	4	4571606	4571666	4571815	4571994	4571770	268.5	9	269
2	2	3	5129211	5129412	5129467	5129695	5129446	269.5	5	270
2	3	4	1577457	1577642	1577672	1577695	1577617	134	2	134
2	3	4	2103630	2103799	2103989	2104176	2103899	368	11	368
2	3	2	2431447	2431638	2432263	2432791	2432035	984.5	12	985
2	4	2	1138845	1138905	1139077	1139160	1138997	243.5	21	244
2	4	4	1724988	1725687	1726330	1726778	1725946	1216.5	5	1217

2	6	1	1406831	1406962	1409630	1409834	1408314	2835.5	104	2836
2	7	1	2140902	2140949	2141212	2141509	2141143	435	6	435
3	1	3	1958151	1958389	1958402	1958440	1958346	151	4	151
3	1	4	250965	251305	258564	258641	254869	7467.5	190	7468
3	2	2	276341	276357	276394	276455	276387	75.5	3	76
3	2	4	1081240	1081282	1081314	1081467	1081326	129.5	3	130
3	2	3	1515769	1515902	1517414	1517551	1516659	1647	36	1647
3	2	1	4581140	4581413	4582518	4582923	4581999	1444	13	1444
3	3	1	2083858	2084158	2084730	2084855	2084400	784.5	32	785
3	3	1	2086583	2086838	2086932	2087078	2086858	294.5	2	295
3	3	1	4830502	4831120	4831818	4832061	4831375	1128.5	22	1129
3	5	2	162435	162635	166837	166915	164706	4341	54	4341
3	6	1	1263014	1263092	1263164	1263243	1263128	150.5	2	151
3	6	4	2581995	2582082	2582161	2582218	2582114	151	4	151
3	7	3	532552	532597	532612	532631	532598	47	2	47
3	7	3	714501	714627	714682	714777	714647	165.5	4	166
3	7	3	2432818	2433100	2433281	2433337	2433134	350	9	350

Table S10. TSETA outcompetes the NGS-based pipeline for detecting the NCO products in the first QM6a/CBS999.97(*MAT1-1*) ascus. Authentic NCOs are highlighted in yellow.

chr#	Chromosome Length (bp)	Position (bp)	GC tract length (bp)	GC tract marker	APD_start_out	APD_start_in	APD_end_in	APD_end_out	Ramark	Position (bp)	GC tract length (bp)	GC tract marker	APD_start_out	APD_start_in	APD_end_in	APD_end_out
					TSETA						NGS-based pipeline [MUMmer4 and Recombine (v1.2)]					
1	6835803	2841837	168	6	2841732	2841773	2841800	2842041	Authentic NCO	2841836	167	2	2841732	2841773	2841798	2842041
1	6835803	4349992	163	5	4349909	4349911	4349918	4350228	An Indel due to a poly-C and -G tract							
2	6234656	1379384	166	3	1379241	1379360	1379405	1379528	Authentic NCO	1379384	165	3	1379241	1379363	1379405	1379528
2	6234656	4817690	68	2	4817606	4817707	4817710	4817738	An Indel due to a poly-G tract							
2	6234656	4955357	19	5	4955339	4955355	4955360	4955372	An Indel due to a poly-G tract							
3	5311445	1308219	339	27	1308011	1308088	1308375	1308402	Authentic NCO	1308219	339	22	1308011	1308088	1308375	1308402
3	5311445	1581203	116	2	1581077	1581213	1581214	1581307	Authentic NCO	1581203	116	2	1581077	1581212	1581214	1581307
3	5311445	2314738	11	4	2314730	2314734	2314742	2314744	An Indel due to a poly-A and -G tract							
3	5311445	3935255	1041	19	3934647	3934821	3935580	3935970	Authentic NCO	3935255	1041	13	3934647	3934821	3935580	3935970
3	5311445	4101515	385	9	4101219	4101426	4101619	4101796	Authentic NCO	4101515	385	9	4101219	4101426	4101619	4101796
4	4556834	1363135	51	3	1363073	1363147	1363155	1363166	Authentic NCO							
4	4556834	1790509	3	2	1790506	1790509	1790510	1790511	An Indel due to a poly-A and -C tract							
4	4556834	1790513	3	2	1790511	1790513	1790514	1790515	An Indel due to a poly-A and -C tract							

4	4556834	3558827	9	3	3558820	3558825	3558831	3558832	An Indel due to a poly-A and -C tract							
4	4556834	3558857	9	3	3558851	3558854	3558857	3558865	An Indel due to a poly-A and -C tract							
4	4556834	3914233	5	2	3914230	3914232	3914235	3914236	An Indel due to a poly-T tract							
5	4159965	7	11	4	1	1	7	17	telomere							
5	4159965	783456	170	2	783355	783388	783475	783607	Authentic NCO	783456	170	2	783355	783388	783475	783607
5	4159965	2906230	142	3	2906100	2906219	2906235	2906367	Authentic NCO	2906231	140	3	2906100	2906222	2906235	2906367
6	4000387	16382	33	3	16360	16371	16379	16417	telomere							
6	4000387	2042371	759	2	2041331	2042652	2042737	2042764	Authentic NCO	2042371	759	2	2041331	2042652	2042737	2042764
6	4000387	2345006	171	2	2344776	2345065	2345066	2345116	rDNA, An Indel due to a poly-G							
6	4000387	2377073	99	2	2377012	2377035	2377040	2377205	rDNA, An Indel due to a poly-G							
6	4000387	2383990	146	2	2383772	2384061	2384062	2384063	rDNA, An Indel due to a poly-G							
6	4000387	3900903	85	2	3900794	3900927	3900944	3900946	An Indel due to a poly-T tract							
6	4000387	3901276	633	3	3900959	3900960	3900968	3902216	An Indel due to a poly-T tract							

Table S11. Comparison of the mitochondrial genome sequences of CBS999.97(*MAT1-1*) and the 4 representative F1 progeny

CBS999.97(*MAT1-1*)		#1-1	#1-3	#1-7	#1-11	InDel
39,004 bp		39,004 bp	39,004 bp	39,004 bp	39,004 bp	
2613-2614	T-T	TGT	TGT	TGT	TGT	Insertion
2632-2634	GAA	G-A	G-A	G-A	G-A	Deletion
2739-2741	GAA	G-A	G-A	G-A	G-A	Deletion
2801-2803	TAA	T-A	T-A	T-A	T-A	Deletion
4626-4627	T-A	TAA	TAA	TAA	TAA	Insertion
14047-14048	T-A	TAA	TAA	TAA	TAA	Insertion

Table S12. List of genes in QM6a and CBS999.97(*MAT1-1*) mitochondrial genomes

T. reesei QM6a				*T. reesei* CBS999.97(*MAT1-1*)			
42,139 bp				39,004 bp			
27.2% GC content				27.3% GC content			
start	end	length	gene	start	end	length	gene
The membrane subunits of mitochondrial ATP synthases							
4162	4308	147	atp8	3361	3507	147	atp8
4470	5249	780	atp6	3656	4435	780	atp6
19805	19999	195	atp9	21928	22152	225	atp9
The mitochondrial cytochrome b (cob) and cytochrome c oxidase I-III (cox1-3)							
28249	31792	3544	cob 2 group I introns (ID, IB)	28089	31612	3524	cob 2 group I introns (ID, IB)
7684	8493	810	cox3	6873	7682	810	cox3
21304	24573	3270	cox2 2 group I introns (IC2, ID)	23752	24435	195	cox2
32470	41101	8632	cox1 5 group I introns (5 IBs)	32292	36038	3747	cox1 1 group I intron (IB)
The membrane subunits of mitochondrial NADH dehydrogenase complex							
882	2339	1458	nad4	13	1470	1458	nad4
8851	9603	753	nad6	8022	8774	753	nad6
17517	19184	1668	nad2	18350	20017	1668	nad2
19185	19598	414	nad3	21394	21720	327	nad3
24920	25189	270	nad4L	24764	25033	270	nad4L
25189	27267	2079	nad5	25033	27111	2079	nad5
41733	42128	396	nad1	36643	38843	2201	nad1
The mitochondrial tRNA genes							
7209	7292	84	tRNA Tyrosine	6395	6478	84	tRNA Tyrosine
7399	7472	74	tRNA Aspartate				
7478	7561	84	tRNA Serine	6667	6750	84	tRNA Serine
7566	7637	72	tRNA Asparagine	6755	6826	72	tRNA Asparagine
8611	8681	71	tRNA Glycine	7784	7854	71	tRNA Glycine

9979	10050	72	tRNA Isoleucine	9127	9198	72	tRNA Isoleucine
10078	10164	87	tRNA Serine	9226	9312	87	tRNA Serine
10170	10241	72	tRNA Tryptophan	9318	9389	72	tRNA Tryptophan
10292	10363	72	tRNA Proline	9442	9513	72	tRNA Proline
15197	15267	71	tRNA Threonine	15723	15793	71	tRNA Threonine
15271	15343	73	tRNA Glutamate				
15344	15414	71	tRNA Methionine	15870	15940	71	tRNA Methionine
15560	15632	73	tRNA Methionine	16086	16158	73	tRNA Methionine
15637	15719	83	tRNA Leucine	16163	16245	83	tRNA Leucine
15812	15883	72	tRNA Alanine	16339	16410	72	tRNA Alanine
15889	15961	73	tRNA Phenylalanine	16416	16488	73	tRNA Phenylalanine
15962	16034	73	tRNA Lysine	16489	16561	73	tRNA Lysine
16112	16195	84	tRNA Leucine	16639	16722	84	tRNA Leucine
16955	17027	73	tRNA Glutamine	17763	17835	73	tRNA Glutamine
17201	17274	74	tRNA Histidine	18036	18109	74	tRNA Histidine
17407	17478	72	tRNA Methionine	18240	18311	72	tRNA Methionine
24695	24765	71	tRNA Arginine	24554	24624	71	tRNA Arginine
31908	31979	72	tRNA Cysteine	31724	31795	72	tRNA Cysteine
41217	41287	71	tRNA Arginine	36154	36224	71	tRNA Arginine
Open reading frames (orfs)							
2688	3608	921	orf306; LAGLIDADG	1812	2720	909	orf302; LAGLIDADG
13113	14531	1419	orf472	10710	11504	795	orf264; GIY
20363	21067	705	orf234; GIY	13665	14063	399	orf132
21385	22689	1305	orf434; LAGLIDADG	14093	15052	960	orf319
23017	23835	819	orf272	20018	21346	1329	orf442
27575	28021	447	orf148	20021	21346	1326	orf441; LAGLIDADG
28642	29523	882	orf293; GIY	22219	23715	1497	orf498; LAGLIDADG
30070	31032	963	orf320; LAGLIDADG	27419	27865	447	orf148
32863	34020	1158	orf385; LAGLIDADG	28482	29354	873	orf290; GIY
34373	35449	1077	orf358; LAGLIDADG	29895	30857	963	orf320; LAGLIDADG
35814	36863	1050	orf349; LAGLIDADG	33417	34493	1077	orf358; LAGLIDADG

38478	39548	1071	orf356; LAGLIDADG	38040	38342	303	orf100; GIY
The mitochondrial rRNA genes							
5659	7167	1509	small subunit rRNA (rns)	4845	6351	1507	small subunit rRNA (rns) rns

Table S13. Variants among the 16 F1 progeny of ascus #1 (each genetically identical group is represented by a different color)

#SNP #InDel #APD	#1-1	#1-2	#1-14	#1-15	#1-3	#1-4	#1-5	#1-6	#1-7	#1-8	#1-9	#1-10	#1-11	#1-12	#1-13	#1-16
#1-1		27 157 184	25 150 175	20 161 181	713239 4345339 5058578	711284 4354047 5065331	713311 4345094 5058405	713312 4345154 5058466	711779 3854774 4566553	711780 3854790 4566570	711786 3854786 4566572	711786 3854778 4566564	563872 1888845 2452717	563868 1888885 2452753	563873 1888851 2452724	563866 1888882 2452748
#1-2			24 137 161	21 134 155	716404 4337562 5053966	714232 4347574 5061806	716424 4337407 5053831	716269 4338677 5054946	706440 3887097 4593537	706488 3886929 4593417	706447 3887101 4593548	706453 3887097 4593550	563940 1889132 2453072	563935 1889168 2453103	563941 1889138 2453079	563939 1889165 2453104
#1-14				17 165 182	703109 4363235 5066344	705607 4349113 5054720	705512 4349470 5054982	705528 4349514 5055042	709696 3850024 4559720	709696 3850036 4559732	709697 3850034 4559731	709708 3850024 4559732	564111 1888377 2452488	564112 1888411 2452523	564110 1888383 2452493	563962 1889144 2453106
#1-15					704879 4354740 5059619	705637 4353492 5059129	705569 4353839 5059408	705528 4349497 5055025	702416 3884007 4586423	702471 3883799 4586270	702420 3884019 4586439	702421 3884011 4586432	564109 1888334 2452443	564107 1888372 2452479	564112 1888338 2452450	563888 1888909 2452797
#1-3						31 122 153	42 169 211	34 101 135	564178 1952197 2516375	564177 1952207 2516384	564175 1952201 2516376	564185 1952205 2516390	707930 3809776 4517706	707796 3805446 4513242	709214 3805958 4515172	706959 3815537 4522496
#1-4							30 111 141	25 47 72	564189 1952329 2516518	564189 1952339 2516528	564189 1952331 2516520	564197 1952335 2516532	707550 3800448 4507998	707471 3800470 4507941	702557 3833228 4535785	706628 3810569 4517197
#1-5								30 100 130	564188 1952268 2516456	564187 1952278 2516465	564178 1952274 2516452	564186 1952278 2516464	706396 3805763 4512159	706314 3805791 4512105	705474 3815905 4521379	705469 3815892 4521361
#1-6									564195 1952264 2516459	564192 1952274 2516466	564183 1952268 2516451	564189 1952272 2516461	706232 3814419 4520651	710692 3788273 4498965	705310 3824559 4529869	709856 3798292 4508148
#1-7										9 42 51	18 54 72	17 50 67	698231 4480635 5178866	699161 4469729 5168890	700433 4466727 5167160	698252 4480546 5178798
#1-8											23 58 81	20 46 66	698239 4480631 5178870	699171 4469725 5168896	700443 4466723 5167166	698271 4480542 5178813
#1-9												13 46 59	698233 4480635 5178868	699165 4469729 5168894	700437 4466727 5167164	698253 4480546 5178799

#1-10			698234 4480625 5178859	699166 4469719 5168885	700438 4466717 5167155	698255 4480536 5178791
#1-11				12 260 272	12 270 282	9 183 192
#1-12					8 308 316	10 373 383
#1-13						17 179 196
#1-16						

Table S14. Application of the NGS-based approach to detect the GC tract lengths in all CO and NCO products generated by QM6a/CBS999.97(*MAT1-1*) hybrid meiosis

CO/NCO	Ascus number	Chromosome number	chr_len	position (bp)	type	GC tract length	APD_start_out	APD_start_in	APD_end_in	APD_end_out
CO	1	1	6835803	290545	CO w/ GC	313	290360	290417	290660	290742
CO	1	1	6835803	1376408	CO w/ GC	280	1376466	1376630	1376220	1376316
CO	1	1	6835803	2846616	CO	192	2846520	2846712	2846520	2846712
CO	1	1	6835803	4850122	CO	163	4850040	4850203	4850040	4850203
CO	1	1	6835803	5942633	CO w/ GC	45	5942600	5942621	5942621	5942690
CO	1	2	6234656	1078314	CO w/ GC	265	1078135	1078229	1078313	1078580
CO	1	2	6234656	3067880	CO w/ GC	290	3067988	3068061	3067677	3067793
CO	1	2	6234656	4581277	CO	273	4581140	4581413	4581140	4581413
CO	1	3	5311445	389221	CO w/ GC	78	389234	389285	389129	389234
CO	1	3	5311445	1639304	CO w/ GC	149	1639259	1639497	1639199	1639259
CO	1	3	5311445	2230879	CO	438	2230660	2231098	2230660	2231098
CO	1	4	4556834	823739	CO	75	823701	823776	823701	823776
CO	1	4	4556834	1922011	CO w/ GC	290	1922088	1922223	1921803	1921929
CO	1	4	4556834	3937471	CO w/ GC	185	3937229	3937528	3937528	3937598
CO	1	5	4159965	906317	CO w/ GC	84	906203	906347	906347	906371
CO	1	5	4159965	1651350	CO w/ GC	112	1651260	1651328	1651328	1651483
CO	1	5	4159965	2640861	CO w/ GC	176	2640809	2641088	2640737	2640809
CO	1	5	4159965	3965025	CO	349	3964850	3965199	3964850	3965199
CO	1	6	4000387	640823	CO w/ GC	309	640643	640693	640864	641090
CO	1	6	4000387	2245856	CO	476	2245618	2246094	2245618	2246094

CO	1	6	4000387	3266023	CO w/ GC	167	3265860	3266018	3266018	3266194
CO	1	7	3823438	1180772	CO	373	1180585	1180958	1180585	1180958
CO	1	7	3823438	2891266	CO w/ GC	661	2890900	2890971	2891551	2891642
CO	1	7	3823438	3411537	CO w/ GC	251	3411387	3411435	3411632	3411692
CO	2	1	6835803	442660	CO w/ GC	183	442558	442580	442608	442895
CO	2	1	6835803	1506686	CO w/ GC	177	1506474	1506720	1506745	1506803
CO	2	1	6835803	2084714	CO	46	2084691	2084737	2084691	2084737
CO	2	1	6835803	4251534	CO w/ GC	370	4251294	4251404	4251501	4251936
CO	2	1	6835803	5974853	CO	255	5974725	5974980	5974725	5974980
CO	2	2	6234656	1674609	CO	681	1674268	1674949	1674268	1674949
CO	2	2	6234656	3361095	CO w/ GC	228	3360922	3361041	3361146	3361272
CO	2	2	6234656	4300667	CO w/ GC	459	4300767	4301025	4300364	4300510
CO	2	2	6234656	5020065	CO w/ GC	139	5020085	5020184	5019921	5020071
CO	2	3	5311445	514337	CO w/ GC	79	514260	514334	514359	514393
CO	2	3	5311445	1423219	CO	45	1423196	1423241	1423196	1423241
CO	2	3	5311445	2307834	CO w/ GC	263	2307852	2308078	2307631	2307774
CO	2	3	5311445	3159413	CO	225	3159300	3159525	3159300	3159525
CO	2	4	4556834	575881	CO	83	575839	575922	575839	575922
CO	2	4	4556834	2627476	CO w/ GC	375	2627285	2627293	2627636	2627691
CO	2	4	4556834	4085717	CO w/ GC	180	4085711	4085902	4085543	4085711
CO	2	5	4159965	745214	CO	123	745152	745275	745152	745275
CO	2	5	4159965	1725040	CO	368	1724856	1725224	1724856	1725224
CO	2	5	4159965	3666802	CO w/ GC	42	3666820	3666825	3666742	3666820
CO	2	6	4000387	832831	CO w/ GC	544	833048	833157	832423	832694
CO	2	6	4000387	3013187	CO w/ GC	524	3013333	3013564	3012895	3012955
CO	2	7	3823438	1243450	CO w/ GC	245	1243420	1243724	1243241	1243413

CO	2	7	3823438	2211609	CO	127	2211545	2211672	2211545	2211672
CO	2	7	3823438	3111216	CO w/ GC	436	3111332	3111536	3110921	3111076
CO	3	1	6835803	250750	CO w/ GC	771	250116	250612	250965	251305
CO	3	1	6835803	801341	CO	14	801334	801348	801334	801348
CO	3	1	6835803	2704428	CO w/ GC	215	2704304	2704336	2704501	2704569
CO	3	1	6835803	5831682	CO w/ GC	225	5831517	5831622	5831664	5831925
CO	3	2	6234656	423288	CO w/ GC	423	422994	423160	423367	423632
CO	3	2	6234656	1523840	CO w/ GC	10570	1529079	1529171	1518542	1518568
CO	3	2	6234656	1673658	CO w/ GC	264	1673723	1673857	1673488	1673564
CO	3	2	6234656	2538004	CO w/ GC	197	2537986	2538219	2537835	2537976
CO	3	2	6234656	3336022	CO	391	3335826	3336217	3335826	3336217
CO	3	2	6234656	5223333	CO	619	5223023	5223642	5223023	5223642
CO	3	3	5311445	537359	CO	198	537260	537458	537260	537458
CO	3	3	5311445	1395321	CO	223	1395209	1395432	1395209	1395432
CO	3	3	5311445	2086093	CO w/ GC	708	2086346	2086547	2085628	2085849
CO	3	4	4556834	558014	CO	336	557846	558182	557846	558182
CO	3	4	4556834	1902320	CO w/ GC	296	1902383	1902552	1901961	1902383
CO	3	4	4556834	2676814	CO	154	2676737	2676891	2676737	2676891
CO	3	4	4556834	3557828	CO w/ GC	1253	3558403	3558505	3557186	3557217
CO	3	5	4159965	775941	CO w/ GC	289	776022	776148	775763	775830
CO	3	5	4159965	1672593	CO w/ GC	219	1672597	1672807	1672372	1672594
CO	3	5	4159965	2923941	CO w/ GC	175	2923773	2923934	2923997	2924060
CO	3	5	4159965	3953162	CO	340	3952992	3953332	3952992	3953332
CO	3	6	4000387	600939	CO w/ GC	79	600880	600918	600933	601023
CO	3	6	4000387	1444345	CO w/ GC	283	1444127	1444280	1444280	1444692
CO	3	6	4000387	2581272	CO w/ GC	259	2581058	2581227	2581227	2581576

CO	3	6	4000387	3091270	CO w/ GC	493	3091487	3091546	3090941	3091107
CO	3	7	3823438	1092932	CO w/ GC	228	1092936	1093155	1092699	1092936
CO	3	7	3823438	3110136	CO w/ GC	158	3110158	3110271	3109955	3110158
NCO	1	1	6835803	2841836	NCO	167	2841732	2841773	2841798	2842041
NCO	1	2	6835803	1379384	NCO	165	1379241	1379363	1379405	1379528
NCO	1	3	5311445	1308219	NCO	339	1308011	1308088	1308375	1308402
NCO	1	3	5311445	1581203	NCO	116	1581077	1581212	1581214	1581307
NCO	1	3	5311445	3935255	NCO	1041	3934647	3934821	3935580	3935970
NCO	1	3	5311445	4101515	NCO	385	4101219	4101426	4101619	4101796
NCO	1	5	4159965	783456	NCO	170	783355	783388	783475	783607
NCO	1	5	4159965	2906231	NCO	140	2906100	2906222	2906235	2906367
NCO	1	6	4000387	2042371	NCO	759	2041331	2042652	2042737	2042764
NCO	2	1	6835803	1370017	NCO	356	1369629	1370048	1370056	1370333
NCO	2	1	6835803	3651818	NCO	58	3651786	3651791	3651837	3651856
NCO	2	1	6835803	3712471	NCO	336	3712241	3712365	3712549	3712728
NCO	2	2	6234656	1085027	NCO	271	1084839	1084945	1085158	1085167
NCO	2	2	6234656	4571770	NCO	269	4571606	4571666	4571815	4571994
NCO	2	2	6234656	5129446	NCO	270	5129211	5129412	5129467	5129695
NCO	2	3	5311445	1577617	NCO	134	1577457	1577642	1577672	1577695
NCO	2	3	5311445	2103899	NCO	368	2103630	2103799	2103989	2104176
NCO	2	3	5311445	2432035	NCO	985	2431447	2431638	2432263	2432791
NCO	2	4	4556834	1138997	NCO	244	1138845	1138905	1139077	1139160
NCO	2	4	4556834	1725946	NCO	1217	1724988	1725687	1726330	1726778
NCO	2	6	4000387	1408314	NCO	2836	1406831	1406962	1409630	1409834
NCO	2	7	3823438	2141143	NCO	435	2140902	2140949	2141212	2141509
NCO	3	1	6835803	1958346	NCO	151	1958151	1958389	1958402	1958440

NCO	3	1	6835803	254869	NCO	7468	250965	251305	258564	258641
NCO	3	2	6234656	276387	NCO	76	276341	276357	276394	276455
NCO	3	2	6234656	1081326	NCO	130	1081240	1081282	1081314	1081467
NCO	3	2	6234656	1516659	NCO	1647	1515769	1515902	1517414	1517551
NCO	3	2	6234656	4581999	NCO	1444	4581140	4581413	4582518	4582923
NCO	3	3	5311445	2084400	NCO	785	2083858	2084158	2084730	2084855
NCO	3	3	5311445	2086858	NCO	295	2086583	2086838	2086932	2087078
NCO	3	3	5311445	4831375	NCO	1129	4830502	4831120	4831818	4832061
NCO	3	5	4159965	164706	NCO	4341	162435	162635	166837	166915
NCO	3	6	4000387	1263128	NCO	151	1263014	1263092	1263164	1263243
NCO	3	6	4000387	2582114	NCO	151	2581995	2582082	2582161	2582218
NCO	3	7	3823438	532598	NCO	47	532552	532597	532612	532631
NCO	3	7	3823438	714647	NCO	166	714501	714627	714682	714777
NCO	3	7	3823438	2433134	NCO	350	2432818	2433100	2433281	2433337
NCO	1	3	5311445	3118049	NCO	155	3117969	3117975	3117984	3118269
NCO	1	6	4000387	2042371	NCO	759	2041331	2042652	2042737	2042764

Table S15. APD density in the CO-associated GC tracts

strain	number			accumulate %		
	T.reesei QM6a/CBS999.97(*MAT1-1*)	*S. cerevisiae* S288c/SK1	*S. cerevisiae* hed1_dmc1	*T.reesei* QM6a/CBS999.97(*MAT1-1*)	*S. cerevisiae* S288c/SK1	*S. cerevisiae* hed1_dmc1
< 2.5	0	215	100	0	17.02296	19.01141
< 5	4	658	283	8	52.09818	53.80228
< 7.5	9	1007	429	18	79.7308	81.55894
< 10	14	1174	496	28	92.95329	94.29658
< 12.5	18	1220	511	36	96.59541	97.14829
< 15	20	1237	517	40	97.94141	98.28897
< 17.5	25	1250	524	50	98.9707	99.61977
< 20	29	1258	525	58	99.60412	99.80989
< 30	35	1262	526	70	99.92082	100
< 40	39	1263	526	78	100	100
< 50	41	1263	526	82	100	100
≥ 50	9	0	0	100	100	100
Total	50	1263	526	100%	100%	100%

Table S16. Chromosomal locations of *T. reesei* genes encoding Rad51 and its associated accessory factors

Gene_id	chr	feature	start	end	Strand	Gene name	Li et al. (1)	*S. cerevisiae*		*N. crassa*		*S. pombe*	
								SGD	name	ID	name	ID	*name*
TRQ_006087	ChI_QM6a	gene	2418506	2419679	+	Rad51							
TRC2_000904	Ch1_CBS1-2	gene	2517125	2518882	+	Rad51	TrA0810W	YER095W	*RAD51*	NCU02741	*mei-3*	SPAC644.14c	*rad51*
TRC1_000914	Ch1_CBS1-1	gene	2517118	2518876	+	Rad51							
TRQ_005882	ChI_QM6a	gene	1828438	1829302	-	Rad52							
TRC2_000688	Ch1_CBS1-2	gene	1908385	1910789	-	Rad52	TrA0616C	YML032C	*RAD52*	NCU04275	*mus-11*	SPAC30D11.10	*rad52*
TRC1_000698	Ch1_CBS1-1	gene	1908385	1910789	-	Rad52							
TRQ_002377	ChII_QM6a	gene	2114507	2116970	+	Rad54							
TRC2_003090	Ch2_CBS1-2	gene	2073273	2076051	+	Rad54	TrB0667W	YGL163C	*RAD54*	NCU02348	*mus-25*	SPAC15A10.03c	*rad54*
TRC1_003112	Ch2_CBS1-1	gene	2073255	2076033	+	Rad54							
TRQ_000947	ChIII_QM6a	gene	3130215	3132636	+	Rad55							
TRC2_005489	Ch3_CBS1-2	gene	3085609	3087862	+	Rad55	TrC0906W	YDR076W	*RAD55*	NCU08806	-	SPAC3C7.03c	*rad55*
TRC1_005351	Ch3_CBS1-1	gene	3085565	3087818	+	Rad55							
TRQ_000401	ChIII_QM6a	gene	1291996	1295418	-	Rad57							
TRC2_004932	Ch3_CBS1-2	gene	1231087	1233385	-	Rad57	TrC0394C	YDR004W	*RAD57*	NCU01771	-	SPAC20H4.07	*rad57*
TRC1_004783	Ch3_CBS1-1	gene	1231052	1233350	-	Rad57							

Table S17. The dissociation rates (mean±SEM) determined from Figure 5.

	*Sc*Dmc1 (1/min)	*Sc*Rad51 (1/min)	*Tr*Rad51 (1/min)
15 nt Homo	0.021±0.001	0.019±0.002	0.025±0.001
15 nt Mis	0.027±0.001	0.031±0.001	0.029±0.001
12 nt Homo	0.050±0.003	0.029±0.002	0.056±0.004

Table S18. List of *S. cerevisiae* strains used in this study.

Name	Genetic background	Genotype	Reference
ORT7235	S288c	*MATα arg4-Bgl his3Δ200 leu2Δ0 lys2Δ0 met15Δ0 trp1Δ63 ura3Δ0*	(24)
ORT7237	SK1	*MATa arg4-RV his4B::LEU2 leu2::hisG lys2 trp1::hisG ura3Δ(PstI-SmaI)::hisG*	(24)
AND1702	S288c/SK1	*MATα/MATa arg4-Bgl/arg4-RV his3Δ200/HIS3 HIS4/his4B::LEU2 leu2Δ0/leu2::hisG lys2Δ0/lys2 met15Δ0/MET15 trp1Δ63/trp1::hisG ura3Δ0/ura3Δ(PstI-SmaI)::hisG*	(24)
NH2294	S288c/SK1	as AND1702, but *dmc1Δ::kanMX6/" hed1Δ::hphMX4/"*	(5)
NHY4723	SK1	*MATa ho::hisG ura3Δ(PstI-SmaI)::hisG leu2::hisG ERG1-(SpeI) his4-X::LEU2-(NgoMIV; +ori)-URA3*	(25)
WHY13283	SK1	as NHY4723, but *rad51Δ::hphMX4*	(26)
WHY13723	S288c/SK1	as AND1702, but *RAD51::natMX4/"*	This work
WHY13731	S288c/SK1	as NH2294, but *RAD51::natMX4/"*	This work
WHY13725	S288c/SK1	as AND1702, but *rad51-trL1::natMX4/"*	This work
WHY13733	S288c/SK1	as NH2294, but *rad51-trL1::natMX4/"*	This work
WHY13727	S288c/SK1	as AND1702, but *rad51-trL2::natMX4/"*	This work
WHY13735	S288c/SK1	as NH2294, but *rad51-trL2::natMX4/"*	This work
WHY13729	S288c/SK1	as AND1702, but *rad51-trL1L2::natMX4/"*	This work
WHY13737	S288c/SK1	as NH2294, but *rad51-trL1L2::natMX4/"*	This work
WHY13843	S288c/SK1	as AND1702, but *rad51-S291T::natMX4/"*	This work
WHY13844	S288c/SK1	as NH2294, but *rad51-S291T::natMX4/"*	This work
WHY13853	S288c/SK1	as AND1702, but *rad51-S291T-trL2::natMX4/"*	This work
WHY13855	S288c/SK1	as NH2294, but *rad51-S291T-trL2::natMX4/"*	This work
WHY13865	S288c/SK1	as AND1702, but *rad51-A298N::natMX4/"*	This work
WHY13867	S288c/SK1	as NH2294, but *rad51-A298N::natMX4/"*	This work
WHY13877	S288c/SK1	as AND1702, but *rad51-A298N-trL2::natMX4/"*	This work
WHY13879	S288c/SK1	as NH2294, but *rad51-A298N-trL2::natMX4/"*	This work
WHY13819	S288c/SK1	as AND1702, but *rad51-M301T::natMX4/"*	This work
WHY13821	S288c/SK1	as NH2294, but *rad51-M301T::natMX4/"*	This work
WHY13831	S288c/SK1	as AND1702, but *rad51-M301T-trL2::natMX4/"*	This work

WHY13833	S288c/SK1	as NH2294, but *rad51-M301T-trL2::natMX4/"*	This work
WHY13794	S288c/SK1	as AND1702, but *rad51-M301Q::natMX4/"*	This work
WHY13797	S288c/SK1	as NH2294, but *rad51-M301Q::natMX4/"*	This work
WHY13807	S288c/SK1	as AND1702, but *rad51-M301Q-trL2::natMX4/"*	This work
WHY13809	S288c/SK1	as NH2294, but *rad51-M301Q-trL2::natMX4/"*	This work

The indicated *rad51* mutant alleles with *ADH1* transcription terminator were integrated into each haploid parental strain (SK1 or S288c) to replace the native *RAD51* coding sequence, and the haploid transformants were selected by resistance to nourseothricin conferred by the natMX4 cassette inserted between the *ADH1* transcription terminator and the native transcription terminator of *RAD51*. The amino acid substitutions encoded in the rad51 locus were then confirmed using DNA sequencing. The haploid SK1 and S288c mutants with the indicated rad51 mutation were then mated to make hybrid diploids that are homozygous for the *rad51* mutant allele.
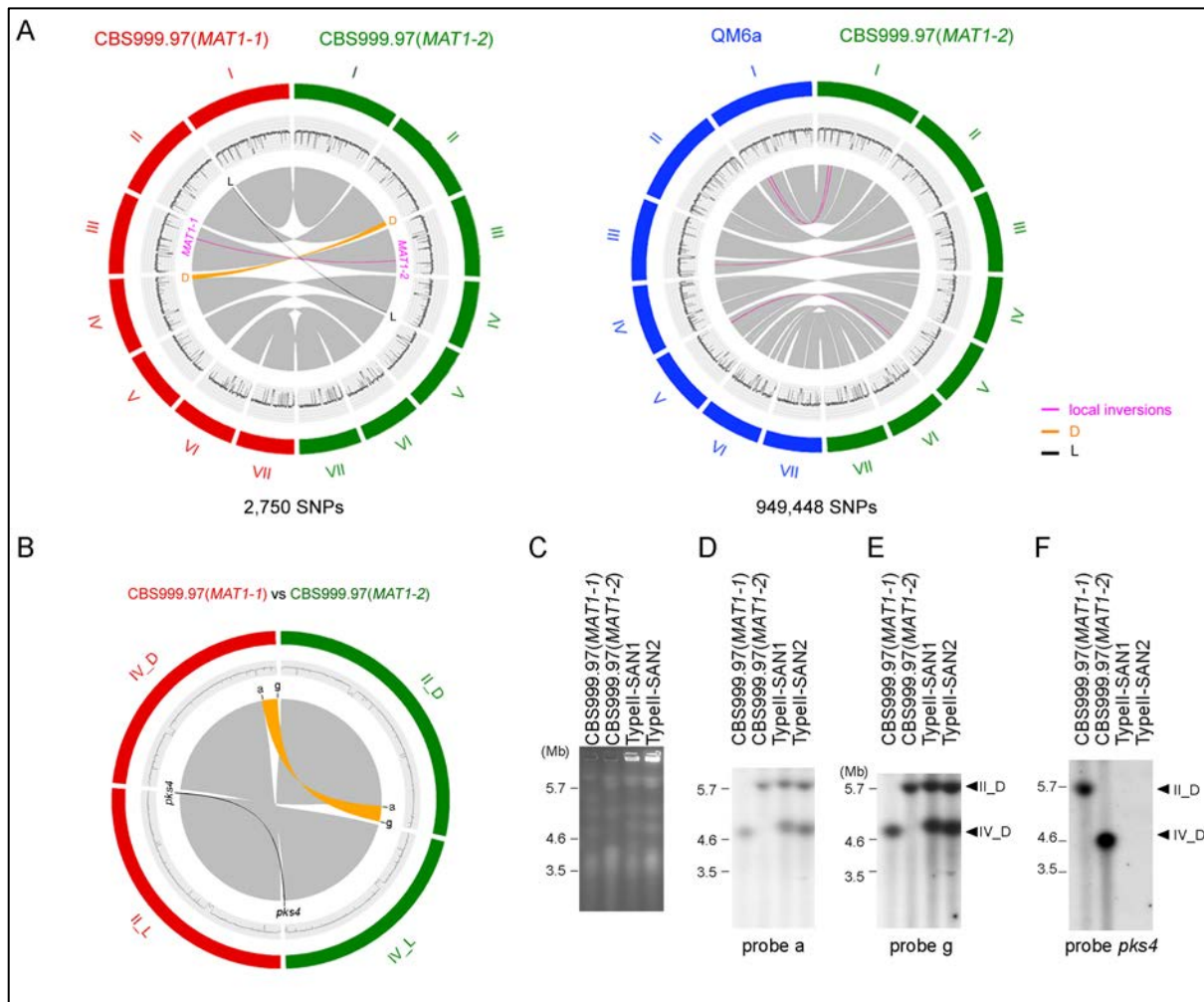
Figure S1. PacBio genome sequencing and assembly. (**A**) Conserved synteny, inversions and translocations between CBS999.97(*MAT1-1*) and CBS999.97(*MAT1-2*) (left-panel) and between QM6a and CBS999.97(*MAT1-2*) (right panel). Collinearity of *T. reesei* genomes is depicted in grey in the inner circles of the diagrams. The D segment is indicated in orange, the L segment in black, and local inversions in magenta. The outer circles indicate the seven chromosomes (I-VII) of CBS999.97(*MAT1-1*) (in red), CBS999.97(*MAT1-2*) (in green) and QM6a (in blue). The GC contents (window size 5000 bp) of the seven chromosomes are shown in the middle traces. (**B**) Reciprocal translocation in CBS999.97(*MAT1-1*). Sexual crosses of CBS999.97(*MAT1-1*) with QM6a or CBS999.97(*MAT1-2*) resulted in ~10% asci with 16 euploid ascospores and ~90% asci with two different types of segmentally aneuploid (SAN) ascospores(1). Using the array-based comparative genome hybridization (aCGH) method, we showed previously that the euploid progeny, as for QM6a and the two CBS999.97 parental strains, germinate to form mycelia with dark-green conidia (i.e., asexual spores). Due to loss of the D segment (~0.5 Mb), type I SAN ascospores cannot germinate. Type II SAN ascospores possess two D segments but lack the L segment (~30 kb). Unlike type I SAN ascospores, type II SAN ascospores can geminate and form mycelia with white conidia(1). The high-quality genome sequences of the three *T. reesei* strains readily confirm the translocation event between the D segment and the L segment. The D segment is indicated in orange, the L segment in black, and local inversions in magenta. The outer circles indicate the two rearranged chromosomes in CBS999.97(*MAT1-1*) (in red) and CBS999.97(*MAT1-2*) (in green). The D segment is located at the right terminus of chromosome II (ChII) in QM6a and CBS999.97(*MAT1-2*) or at the right terminus of chromosome IV (ChIV) in CBS999.97(*MAT1-*

1). In contrast, the L segment is located at the right terminus of ChIV in QM6a and CBS999.97(*MAT1-2*) or at the right terminus of ChII in CBS999.97(*MAT1-1*). CBS999.97(*MAT1-1*) and CBS999.97(*MAT1-2*) were referred to in a previous study(1) as CBS999.97(*MAT1-1*, ChII_L, ChIV_D) and CBS999.97(*MAT1-2*, ChII_D, ChIV_L), respectively. (**C**) Pulsed field gel electrophoresis (PFGE) was applied to separate the seven chromosomes of CBS999.97(*MAT1-1*), CBS999.97(*MAT1-2*) and two type II SAN progeny strains (SAN1 and SAN2). (**c-e**) Southern hybridization with the DNA probes a (**D**) and g (**E**) in the D segment, as well as a DNA probe in the L segment (i.e., *pks4*) (**F**). The results confirmed that CBS999.97(*MAT1-1*) and CBS999.97(*MAT1-2*) contain the D and L segments in the two corresponding chromosomes. In contrast, in SAN1 and SAN2, both ChII and ChIV harbored the D segment but not the L segment (**C-E**). These results provide additional evidence of high-quality genome assembly for these two CBS999.97 haploid strains.
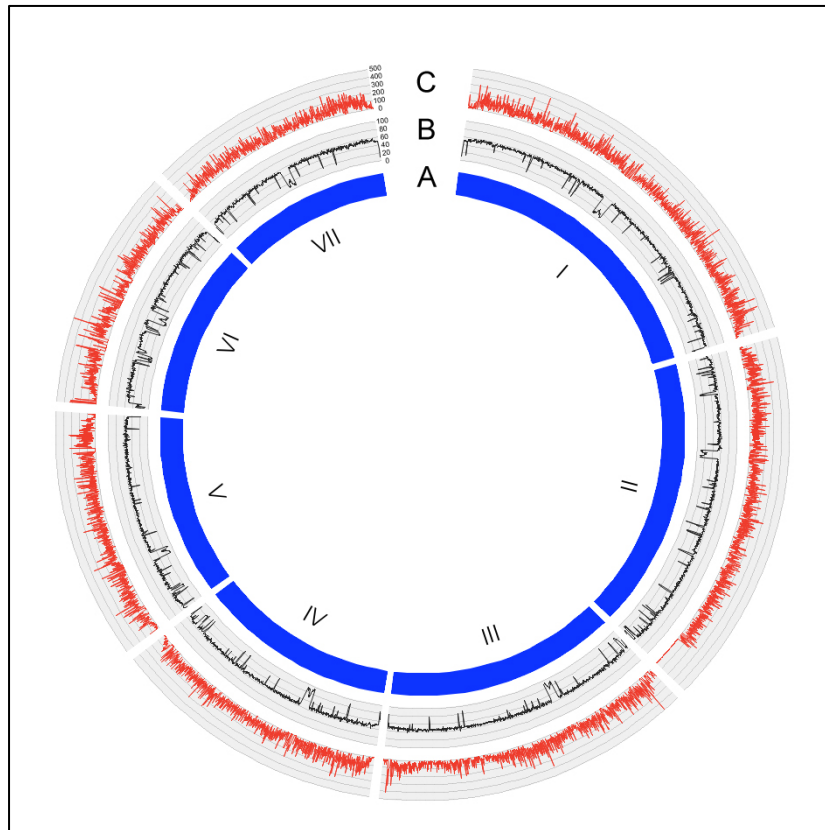
Figure S2. APD markers are evenly distributed throughout the seven chromosomes of QM6a and CBS999.97(*MAT1-1*). CIRCOS was used to visualize the genome-wide APDs revealed by MUMmer4. (A) The karyotype of the QM6a genome (in blue). (B) Guanosine and cytosine (GC) content based on a sliding window of 5000 bp. (C) Variation distribution by chromosome. The APD density between QM6a and CBS999.97(*MAT1-1*) was calculated in a 3-kb window.

Figure S3. Differences in the results of variant calling by TSETA and MUMmer4. Intuitive visualization of the representative chromosome regions [i.e., Ch4: 1363135-1363202 (A) and Ch4: 1139036-1139097 (B)] and divergent variant calling results at single-nucleotide level. Nucleotide sequences of QM6a (in blue) and CBS999.97(*MAT1-1*) (in red) are shown. Three (A) and two (B) short sequence gaps [i.e., null (n) spaces indicated by black arrows] were generated in the two representative chromosome regions by MUMmer4, but not by TSETA, respectively.

Figure S4. Application of the NGS-based variant calling approach to detect *Trichoderma reesei* meiotic recombination products. MUMmer4 was used to genotype APD positions between four representative F1 progeny relative to QM6a and CBS999.97(*MAT1-1*). The results were analyzed in Recombine (v2.1) and GroupEvents (8) to detect CO and NCO products (with ≥2 3:1 and/or 4:0 markers). PlotTetrad (8), a component of Recombine (v2.1), was then used to create graphical representations of all seven chromosomes of the two parental strains and the four representative F1 progeny. QM6a and sequence-identical recombination products are depicted with blue bars and those of CBS999.97(*MAT1-1*) are represented by red bars. Empty areas are highly AT-rich sequences lacking read coverage or APDs. The Illumina NextSeq paired ends from the four representative F1 progeny were used to generate the genome-wide recombination profiles of the three QM6a/CBS999.97(*MAT1-1*) asci (represented in A-C).
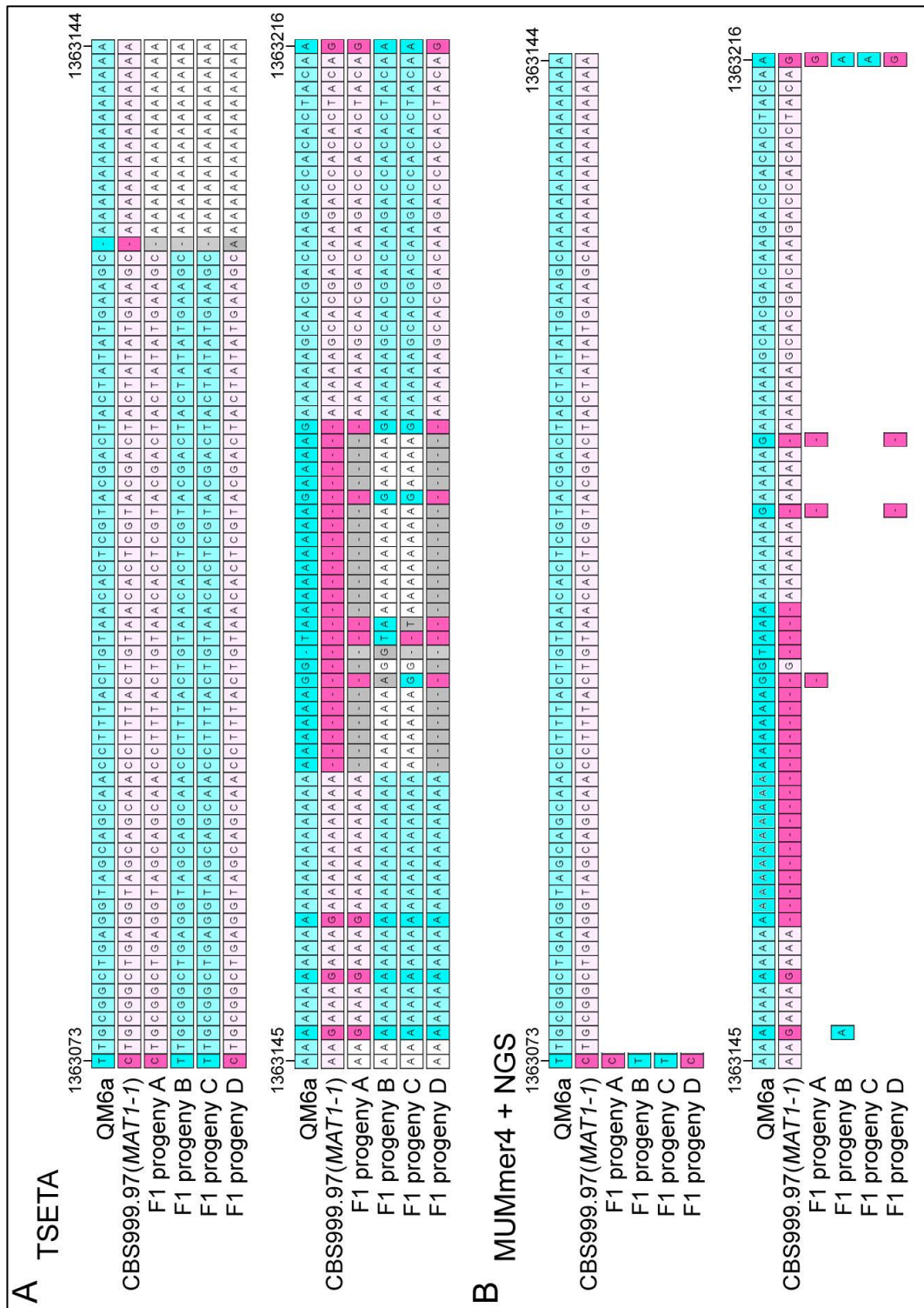
Figure S5. The NCO (with ≥2 APDs and ≥1 SNP) revealed by the "Tetrad" mode of TSETA (A) but not the NGS-based method (B). Intuitive visualization of the two NCO meiotic recombination products at single-nucleotide level. All non-2:2 markers are highlighted in cyan. The NCO product (Ch4: 1363073-1363216) comprise three SNP 1:3 or 3:1 markers and is located within a polyA/T fragment in QM6a. As described in Figure 1A, MUMmer4 (but not TSETA) introduced three short sequence gaps after variant calling. Subsequently, the NGS-based method failed to identify SNPs and/or InDels in the corresponding chromosomal regions of the four representative F1 progeny (B).
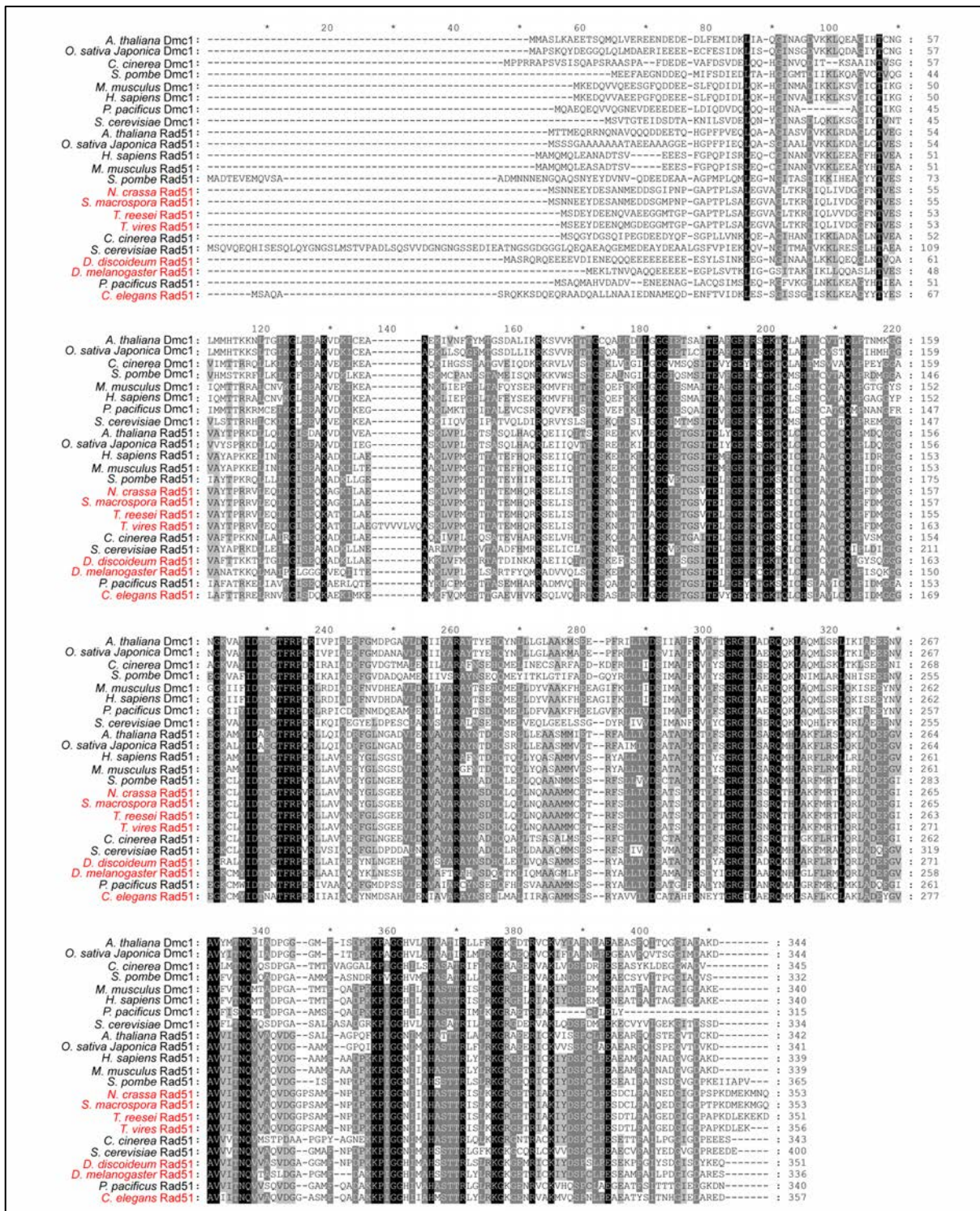
Figure S6. Alignment of the amino acid sequences of Rad51 and Dmc1 from 15 different species. **Alignment of the amino acid sequences of Rad51 and Dmc1 from 15 different species**. Dmc1 was lost in seven Rad51-only eukaryotic organisms (in red). The 15 Rad51 and 8 Dmc1 protein sequences were aligned using ClustalW with default settings in MEGA version 7 (27).
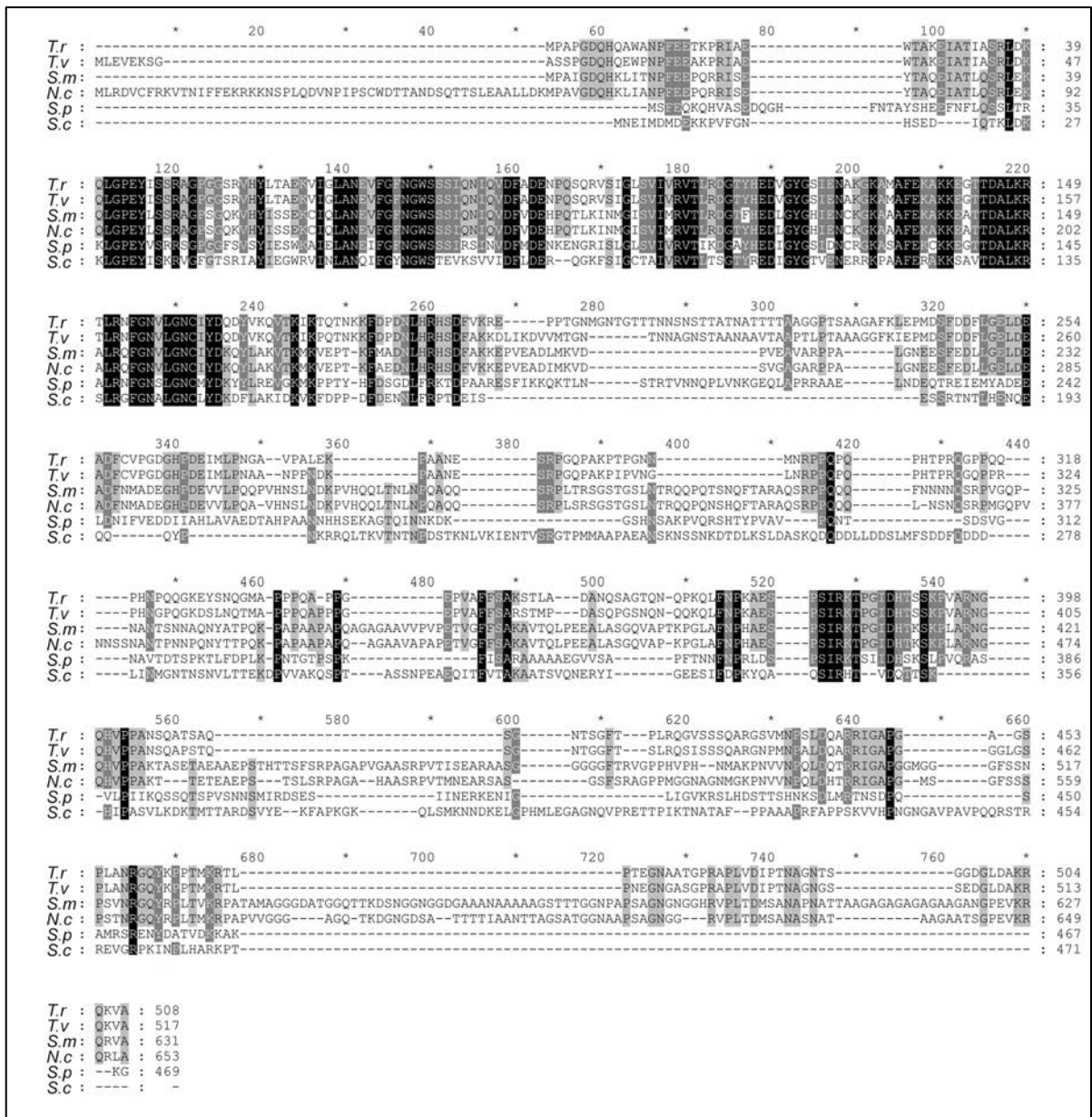
Figure S7. Rad52 homolog sequence alignment. Amino acid sequence alignment of *Trichoderma reesei* (*T.r.*) Rad52 protein with those of *Trichoderma virens* (*T.v.*), *Sordaria macrospora* (*S.m.*), *Neurospora crassa* (*N.c.*), *Schizosaccharomyces pombe* (*S.p.*), and *Saccharomyces cerevisiae* (*S.c.*).
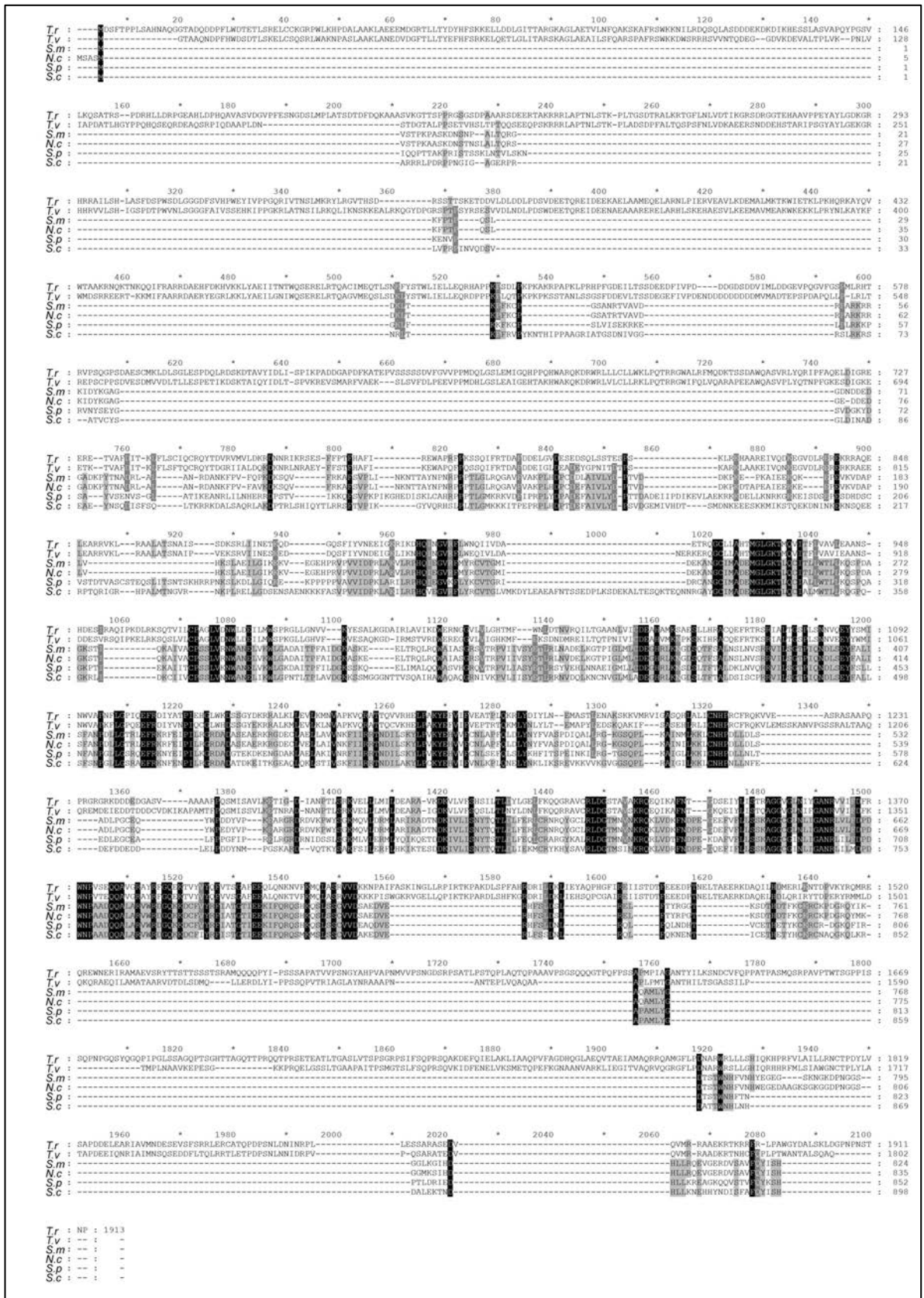
Figure S8. Rad54 homolog sequence alignment. Amino acid sequence alignment of *Trichoderma reesei* (*T.r.*) Rad54 protein with those of *Trichoderma virens* (*T.v.*), *Sordaria macrospora* (*S.m.*), *Neurospora crassa* (*N.c.*), *Schizosaccharomyces pombe* (*S.p.*), and *Saccharomyces cerevisiae* (*S.c.*).

55
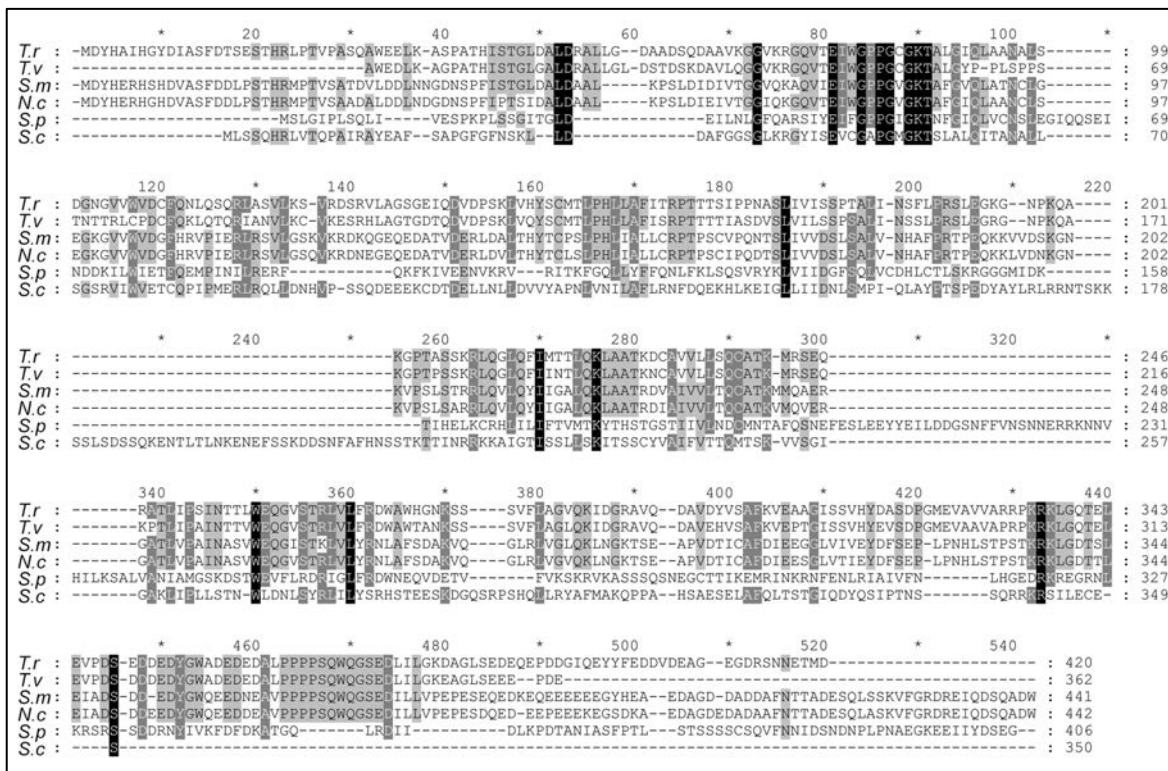
Figure S9. Rad55 homolog sequence alignment. Amino acid sequence alignment of *Trichoderma reesei* (*T.r.*) Rad55 protein with those of *Trichoderma virens* (*T.v.*), *Sordaria macrospora* (*S.m.*), *Neurospora crassa* (*N.c.*), *Schizosaccharomyces pombe* (*S.p.*), and *Saccharomyces cerevisiae* (*S.c.*).
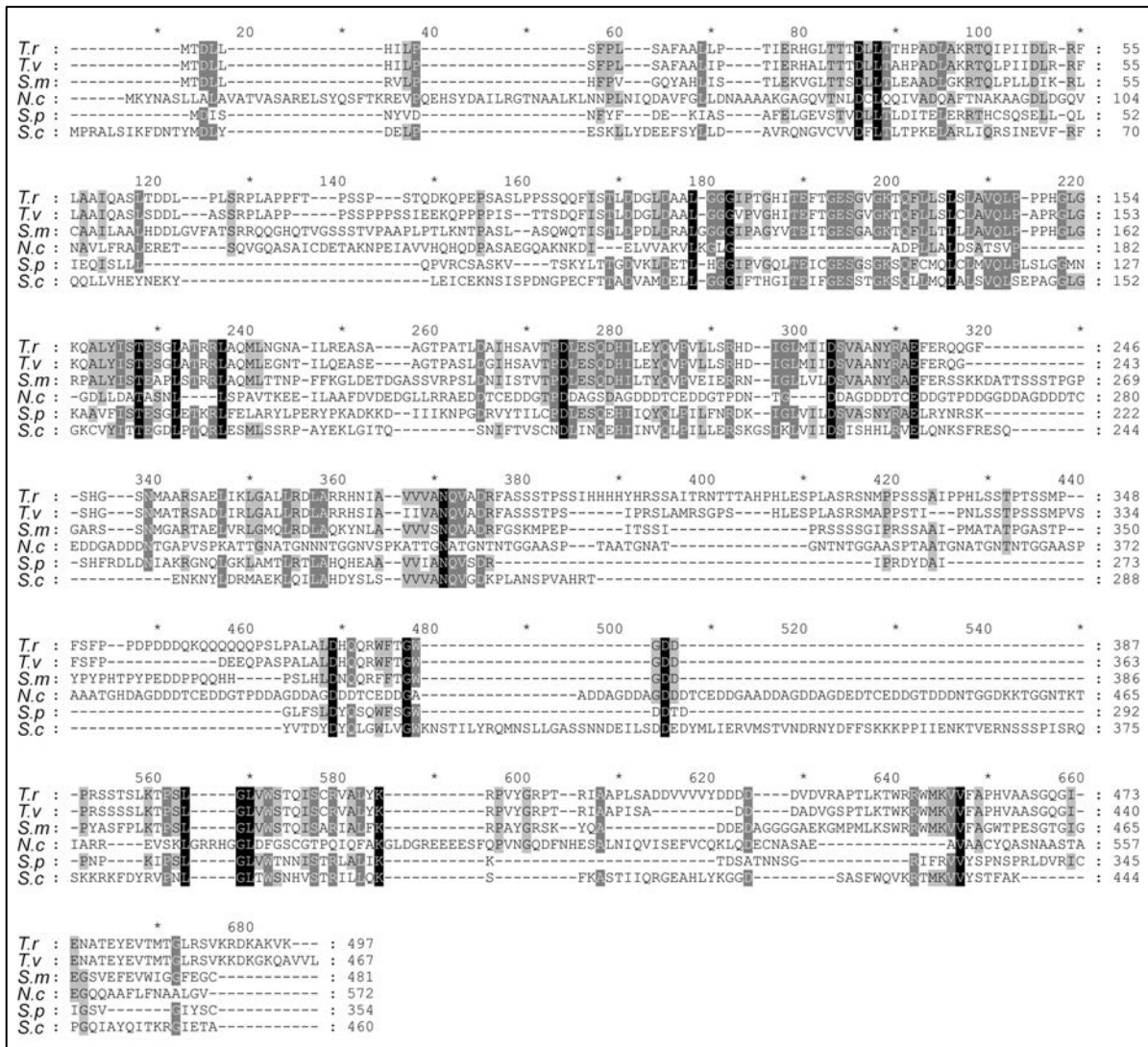
Figure S10. Rad57 homolog sequence alignment. Amino acid sequence alignment of *Trichoderma reesei* (*T.r.*) Rad57 protein with those of *Trichoderma virens* (*T.v.*), *Sordaria macrospora* (*S.m.*), *Neurospora crassa* (*N.c.*), *Schizosaccharomyces pombe* (*S.p.*), and *Saccharomyces cerevisiae* (*S.c.*).
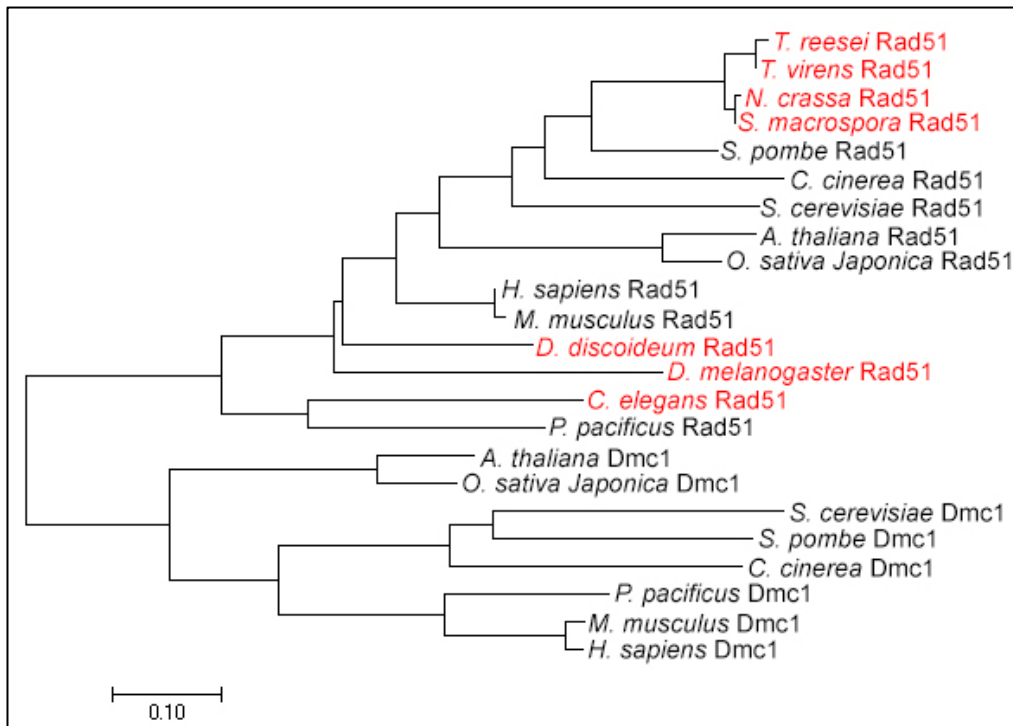
Figure S11. Phylogenetic tree of Rad51 and Dmc1 proteins from 15 different eukaryotic organisms. Dmc1 was lost from the six "Rad51-only" eukaryotic organisms (in red). Evolutionary history was inferred by using a Maximum Likelihood approach and the JTT matrix-based model in MEGA7 (27). The tree is drawn to scale, with branch lengths representing the number of substitutions per site. The analysis involved 23 amino acid sequences. All positions containing gaps and missing data were eliminated. The final dataset represents a total of 290 positions.
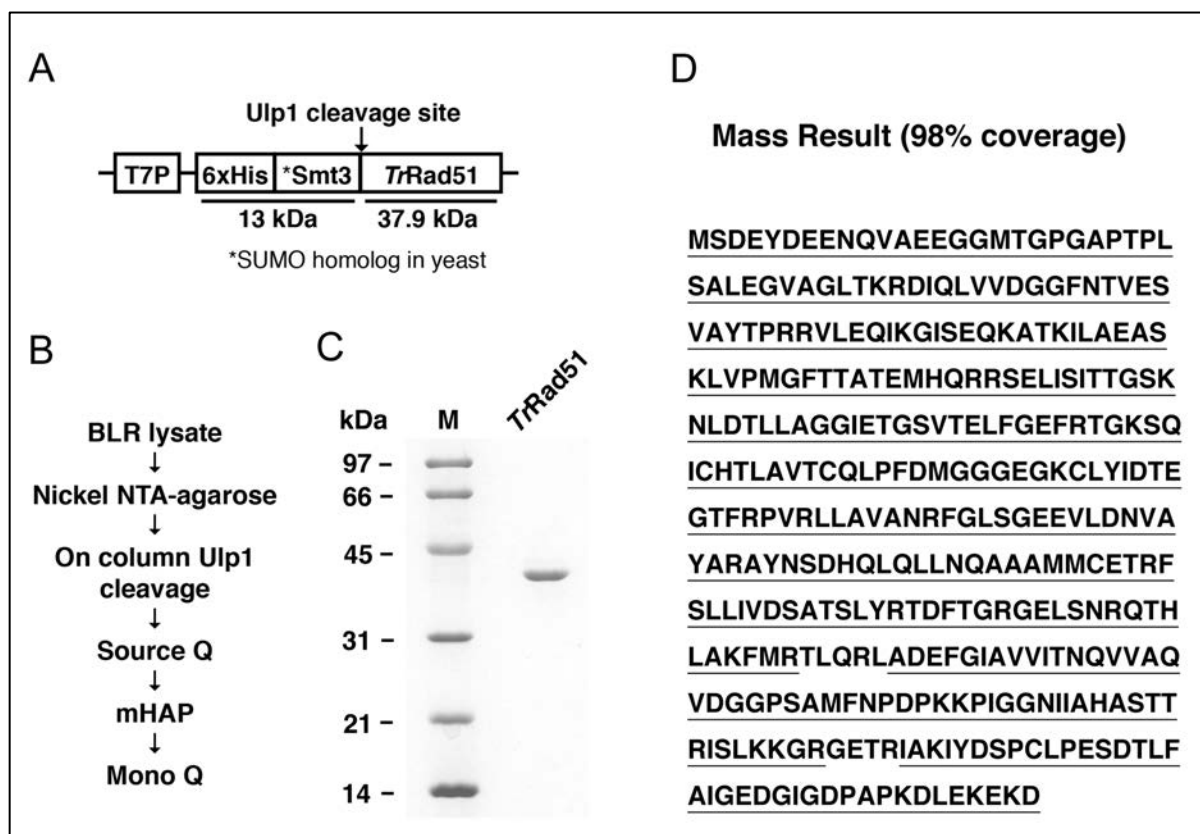
Figure S12. Expression and purification of *Tr*Rad51. (A) Schematic of the (His)$_6$-Smt3-*Tr*Rad51 expression plasmid(4). *Tr*Rad51 was expressed in the *recA*-deficient BLR *E. coli* strain. (B) Schematic of the comprehensive chromatographic procedure we performed for *Tr*Rad51 purification. Details of purification conditions are described in "Materials and Methods". (C) Purified *Tr*Rad51 protein (1.2 μg) was analyzed by 12% SDS-PAGE. (D) The identity of purified protein was further confirmed by MALDI-TOF analysis. The underlined amino acids correspond with the identified fragments of purified *Tr*Rad51.
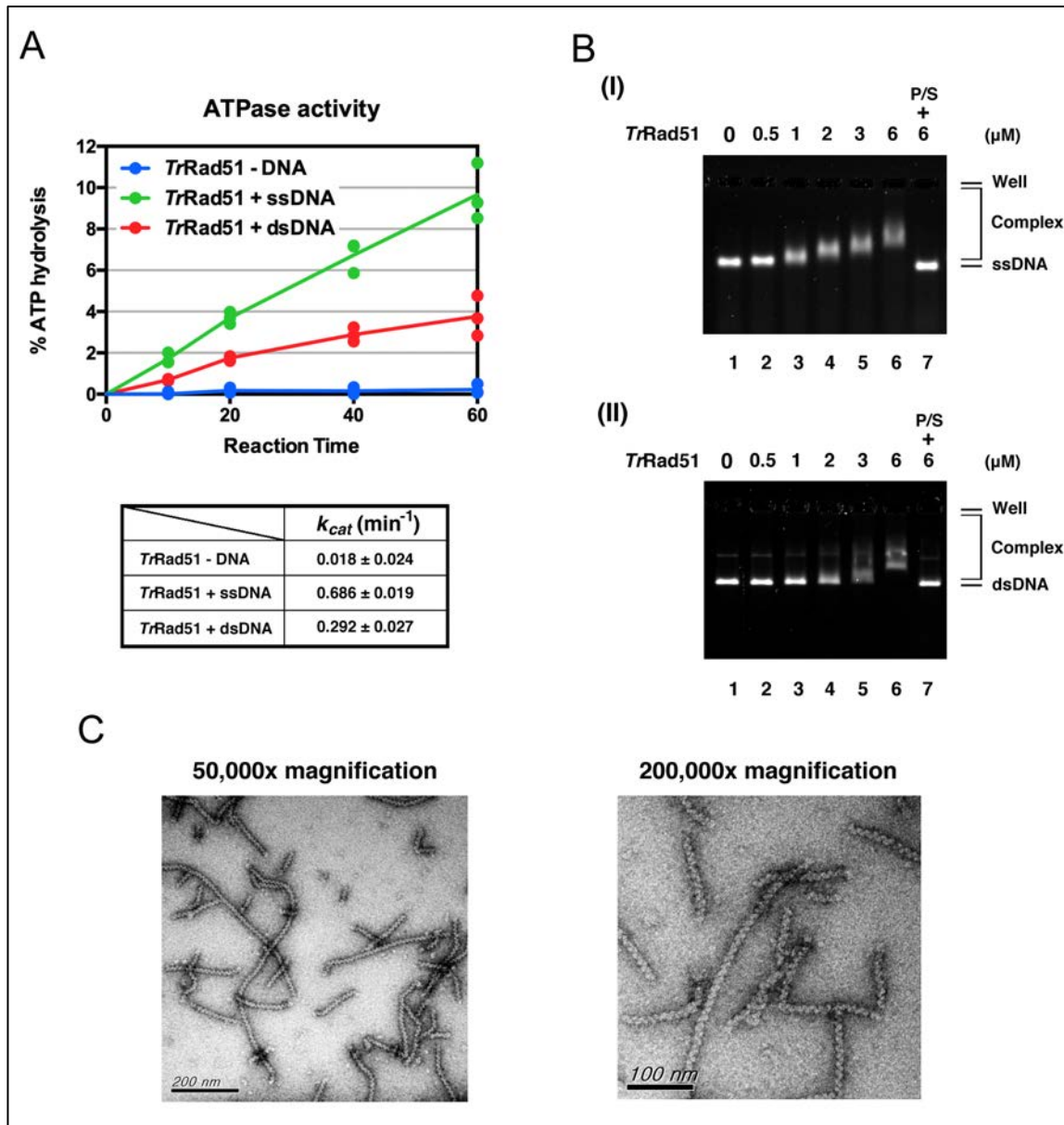
Figure S13. The biochemical and biophysical characteristics of *Tr*Rad51. *Tr*Rad51 possesses the general properties of recombinases, including DNA-stimulated ATPase activity, DNA binding, and the formation of nucleoprotein filament. (A) *Tr*Rad51 (2.5 μM) was incubated with γ-P^{32}-ATP and Φx174 viral (+ sense) ssDNA (15 μM) or linearized dsDNA (15 μM), and then subjected to thin-layer chromatography at the indicated times to monitor ATPase activity. The quantitative data shown are average values ± s.e.m. from three independent experiments. (B) For the DNA mobility shift assay, the indicated concentrations of *Tr*Rad51 was mixed with (I) ssDNA or (II) dsDNA for 30 min to monitor DNA binding. The samples with the highest protein concentration were treated with proteinase K and SDS (P/S) to release DNA. (C) *Tr*Rad51 (0.8 μM) was incubated with 80-mer ssDNA (2.4 μM) for 30 min and nucleoprotein filaments were visualized by electron microscopy.
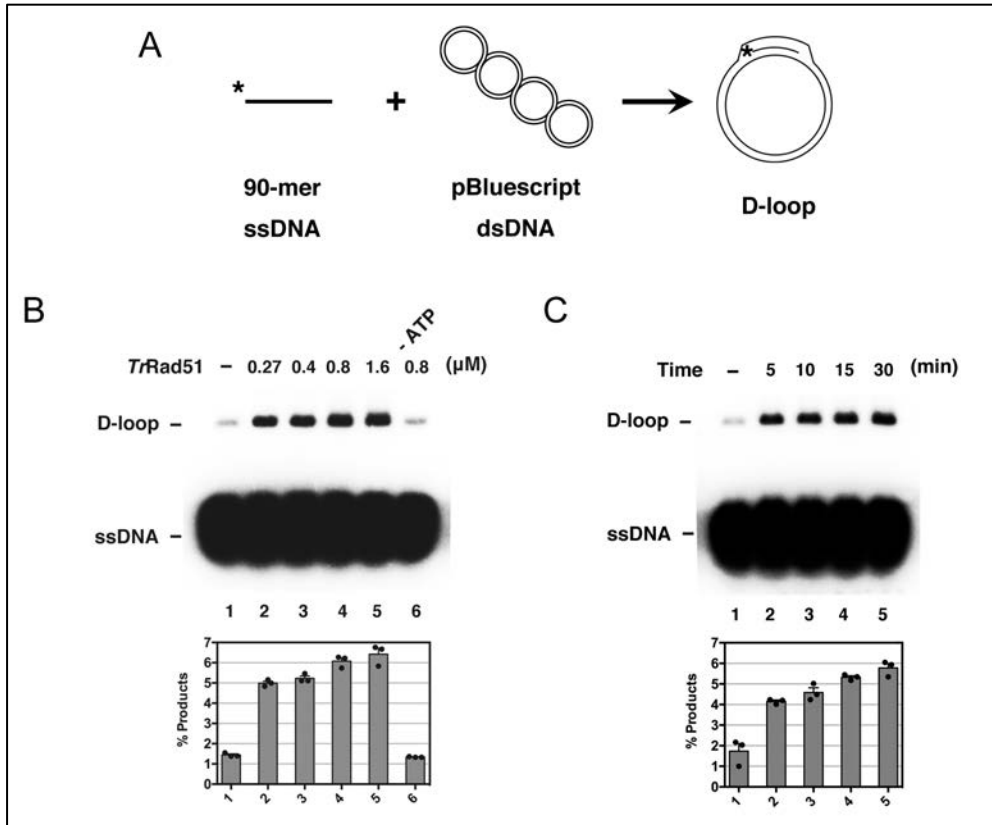
Figure S14. Monitoring *Tr*Rad51 recombinase activity by displacement-loop assay. (A) Schematic of the displacement-loop assay. The ^{32}P-labeled 90-mer ssDNA was pre-incubated with *Tr*Rad51 and addition of dsDNA initiated the reaction. The radiolabeled end products were visualized and quantified by phosphorimaging analysis. (B) Formation of D-loop product at the indicated *Tr*Rad51 protein concentrations was monitored. (C) Formation of D-loop product at the indicated reaction times was monitored. The quantitative data shown are average values ± s.e.m. from three independent experiments.
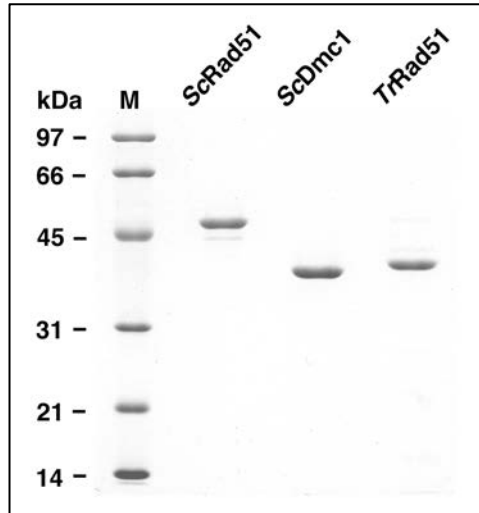
Figure S15. Purified *Sc*Rad51 and *Sc*Dmc1. The purified proteins of *S. cerevisiae* Rad51 and Dmc1 (1.2 μg each) were analyzed by 12% SDS-PAGE to confirm near 95% purity.
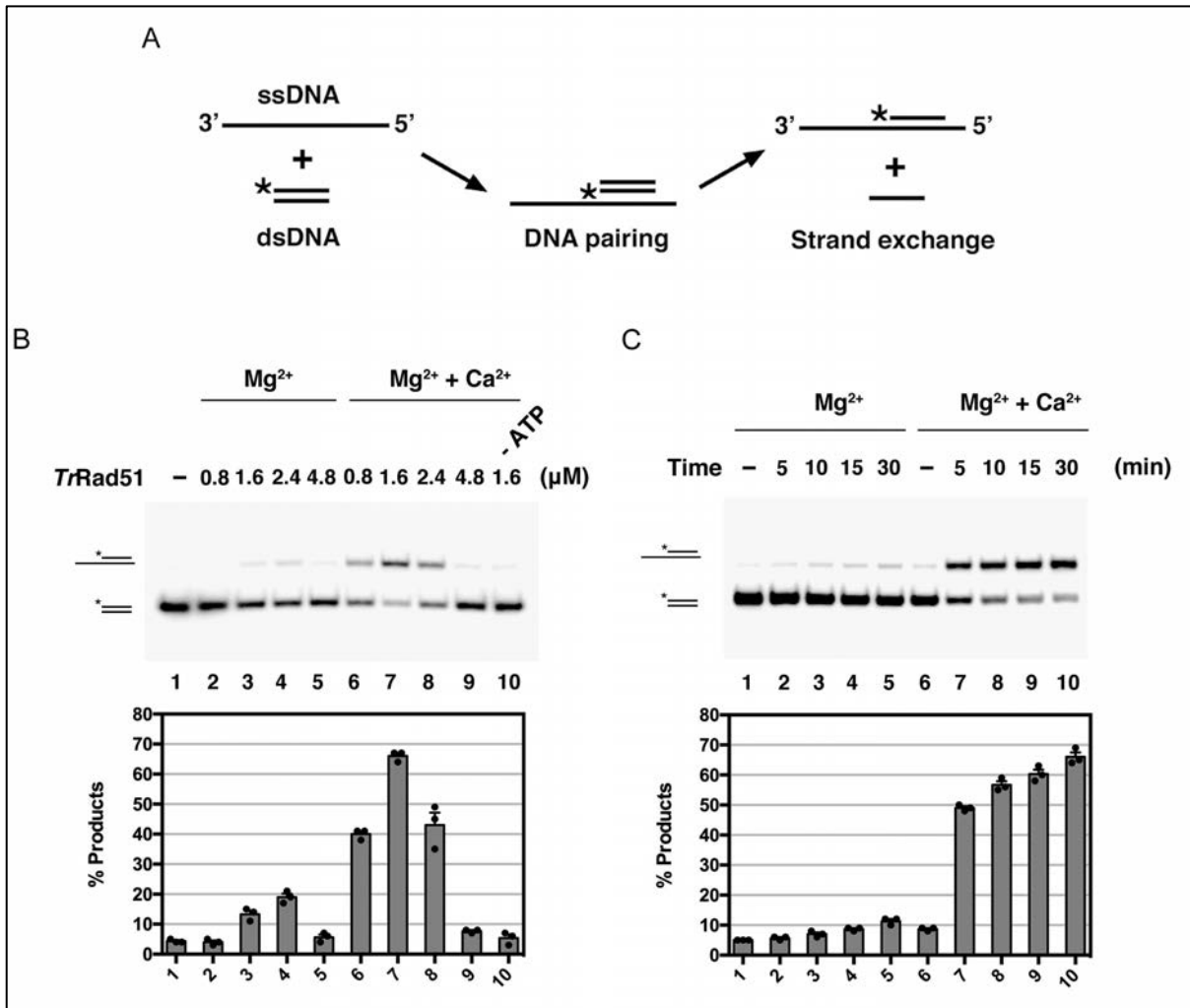
Figure S16. *Tr*Rad51-mediated DNA strand exchange activity. Strand exchange assay demonstrating that *Tr*Rad51 can perform strand exchange and its activity is stimulated in dosage- and time-dependent manners by the addition of calcium. (A) Schematic of the strand exchange assay. The 80-mer ssDNA was pre-incubated with *Tr*Rad51 and addition of ^{32}P-labeled (asterisk) 40-mer dsDNA initiated the reaction. (B), (C) The radiolabeled end products were visualized and quantified by phosphorimaging analysis. The end product of *Tr*Rad51-mediated strand exchange was monitored with or without calcium. Protein concentration (B) or reaction time (C) is indicated. Quantitative data shown are average values ± s.e.m. from three independent experiments.
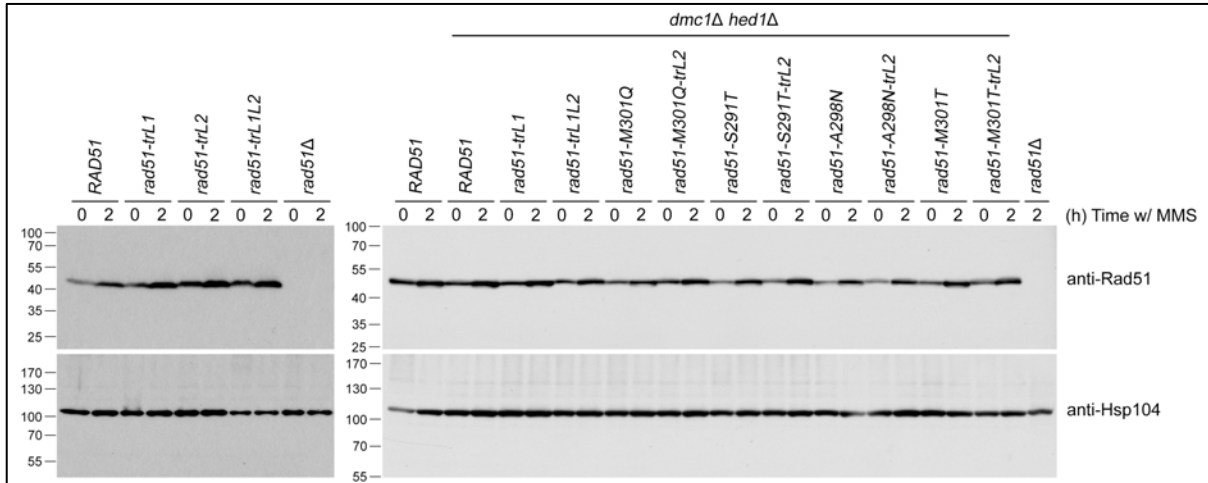
Figure S17. Immunoblotting of WT and mutant *Sc*Rad51 proteins in vegetatively growing cells (*SI* Appendix, Table S18). Yeast strains expressing WT and mutant *Sc*Rad51 proteins were grown in YPD media with or without 0.02% MMS for 2 hours. Total cell lysate of indicated yeast haploid strains was prepared by using the TCA precipitation protocol we developed previously(28). Total proteins were separated by SDS-PAGE. Anti-*Sc*Rad51 antisera were used to visualize *Sc*Rad51 proteins by Western blotting. Hsp104 was used as a loading control.

References:

1. C. L. Chen *et al.*, Blue light acts as a double-edged sword in regulating sexual development of *Hypocrea jecorina* (*Trichoderma reesei*). *PLoS One* **7**, e44969 (2012).

2. Y. C. Chuang *et al.*, *Trichoderma reesei* meiosis generates segmentally aneuploid progeny with higher xylanase-producing capability. *Biotechnol Biofuels* **8**, 30 (2015).

3. W. C. Li *et al.*, *Trichoderma reesei* complete genome sequence, repeat-induced point mutation, and partitioning of CAZyme gene clusters. *Biotechnol Biofuels* **10**, 170 (2017).

4. C. Y. Chen, C. W. Lin, C. Y. Chang, S. T. Jiang, Y. P. Hsueh, Sarm1, a negative regulator of innate immunity, interacts with syndecan-2 and regulates neuronal morphology. *J Cell Biol* **193**, 769-784 (2011).

5. T. L. Callender *et al.*, Mek1 down regulates Rad51 activity during yeast meiosis by phosphorylation of Hed1. *Plos Genet* **12**, e1006226 (2016).

6. A. Herrera-Estrella, G. H. Goldman, M. van Montagu, R. A. Geremia, Electrophoretic karyotype and gene assignment to resolved chromosomes of *Trichoderma spp*. *Mol Microbiol* **7**, 515-521 (1993).

7. G. Marcais *et al.*, MUMmer4: A fast and versatile genome alignment system. *PLoS Comput Biol* **14**, e1005944 (2018).

8. C. M. Anderson *et al.*, ReCombine: a suite of programs for detection and analysis of meiotic recombination in whole-genome datasets. *PLoS One* **6**, e25509 (2011).

9. A. Oke, C. M. Anderson, P. Yam, J. C. Fung, Controlling meiotic recombinational repair - specifying the roles of ZMMs, Sgs1 and Mus81/Mms4 in crossover formation. *Plos Genet* **10**, e1004690 (2014).

10. W. C. Li, H. C. Liu, Y. J. Lin, S. Y. Tung, T. F. Wang, Third-generation sequencing-based mapping and visualization of single nucleotide polymorphism, meiotic

recombination, illegitimate mutation and repeat-induced point mutation *NAR Genomics and Bioinformatics* **2**, lqaa056 (2020).

11. H. C. Liu, W. C. Li, T. F. Wang, TSETA: A Third-generation sequencing-based computational tool for mapping and visualization of SNPs, meiotic recombination products, and RIP mutations. *Methods Mol Biol* **2234**, 331-361 (2021).

12. H. Li *et al.*, The sequence alignment/map format and SAMtools. *Bioinformatics* **25**, 2078-2079 (2009).

13. B. J. Walker *et al.*, Pilon: an integrated tool for comprehensive microbial variant detection and genome assembly improvement. *PLoS One* **9**, e112963 (2014).

14. C. D. Lee *et al.*, An improved SUMO fusion protein system for effective production of native proteins. *Protein Sci* **17**, 1241-1248 (2008).

15. M. Raschle, S. Van Komen, P. Chi, T. Ellenberger, P. Sung, Multiple interactions with the Rad51 recombinase govern the homologous recombination function of Rad54. *J Biol Chem* **279**, 51973-51980 (2004).

16. E. L. Hong, A. Shinohara, D. K. Bishop, *Saccharomyces cerevisiae* Dmc1 protein promotes renaturation of single-strand DNA (ssDNA) and assimilation of ssDNA into homologous super-coiled duplex DNA. *J Biol Chem* **276**, 41906-41912 (2001).

17. V. Busygina *et al.*, Functional attributes of the *Saccharomyces cerevisiae* meiotic recombinase Dmc1. *DNA Repair (Amst)* **12**, 707-712 (2013).

18. C. H. Lu *et al.*, Swi5-Sfr1 stimulates Rad51 recombinase filament assembly by modulating Rad51 dissociation. *Proc Natl Acad Sci U S A* **115**, E10059-E10068 (2018).

19. L. J. Friedman, J. Gelles, Multi-wavelength single-molecule fluorescence analysis of transcription mechanisms. *Methods* **86**, 27-36 (2015).

20. B. Ewing, L. Hillier, M. C. Wendl, P. Green, Base-calling of automated sequencer traces using phred. I. Accuracy assessment. *Genome Res* **8**, 175-185 (1998).

21. F. A. Simao, R. M. Waterhouse, P. Ioannidis, E. V. Kriventseva, E. M. Zdobnov, BUSCO: assessing genome assembly and annotation completeness with single-copy orthologs. *Bioinformatics* **31**, 3210-3212 (2015).

22. E. V. Kriventseva *et al.*, OrthoDB v10: sampling the diversity of animal, plant, fungal, protist, bacterial and viral genomes for evolutionary and functional annotations of orthologs. *Nucleic Acids Res* **47**, D807-D811 (2019).

23. J. Palmer (2017) Funannotate: Fungal genome annotation scripts (https://readthedocs.org/projects/funannotate/downloads/pdf/stable/).

24. R. Laureau, S. Loeillet, F. Salinas, A. Bergström, P. Legoix-Né, G. Liti, A. Nicolas, Extensive recombination of a yeast diploid hybrid through meiotic reversion *Plos Genetics* 12(2): e1005781 (2016)

25. J. P. Lao *et al.*, Meiotic crossover control by concerted action of Rad51-Dmc1 in homolog template bias and robust homeostatic regulation. *Plos Genet* **9**, e1003978 (2013).

26. T. T. Woo, C. N. Chuang, M. Higashide, A. Shinohara, T. F. Wang, Dual roles of yeast Rad51 N-terminal domain in repairing DNA double-strand breaks. *Nucleic Acids Res* **48**, 8474-8489 (2020).

27. S. Kumar, G. Stecher, K. Tamura, MEGA7: Molecular evolutionary genetics analysis version 7.0 for Bigger Datasets. *Mol Biol Evol* **33**, 1870-1874 (2016).

28. C. H. Cheng *et al.*, SUMO modifications control assembly of synaptonemal complex and polycomplex in meiosis of Saccharomyces cerevisiae. *Genes Dev* **20**, 2067-2081 (2006).